Cement and Concrete Research 204 (2026) 108209

Contents lists available at ScienceDirect

Cement and Concrete Research

journal homepage: www.elsevier.com/locate/cemconres

A new approach for exploring the microstructure of low-clinker cements: The role of water mass balance

Aysha Anagreh [a,b,*], Maciej Zajac [a], Mohsen Ben Haha [a], Arnaud Muller [a], Fabien Georget [b], Thomas Matschei [b]

[a] Heidelberg Materials, Global Research & Development, Oberklamweg 2-4, Leimen, 69181, Germany
[b] Institute of Building Materials Research at RWTH Aachen University, Aachen, 52062, Germany

ARTICLE INFO

Keywords:
Low clinker
Water mass balance
Porosity
Calcined clay
Natural pozzolana

ABSTRACT

A comprehensive investigation into the microstructure of low clinker binders with cement content below 45% is fundamental for understanding the mechanisms governing their mechanical and durability performances in practical applications. This study introduces a novel water mass balance approach to characterize the complex microstructure of low clinker binders, incorporating limestone and calcined clay or natural pozzolana at varying replacement levels. The approach quantifies water content and its distribution across different hydration products and pore sizes, integrating multiple analytical techniques to provide a deep understanding of the microstructural evolution. The interlayer and gel water contents of the natural pozzolana mixtures calculated from DVS measurement reflect the solid volume of C-(A)-S-H gel phases. In contrast, calcined clay mixtures exhibit inconsistencies interlayer and gel water associated with C-(A)-S-H gel, likely due to the limited availability of saturated spaces at later ages and the inherent complexity of the calcined clay material. Despite individual uncertainties, the combined techniques yield consistent water quantification across the hydrated systems.

1. Introduction

One viable pathway to reducing the cement and concrete industry emissions is the use of low clinker cements, where supplementary cementitious materials (SCMs) such as, fly ash, granulated blast furnace slag, calcined clay and limestone partially replace clinker [1]. However, the availability of fly ash and slag is reducing due to the limited sources and the change of production path [2,3]. Therefore, the global study and production of SCMs is now focusing on natural pozzolana and the synergetic impact of calcined clay and limestone [3]. It was proven that limestone calcined clay cement, with kaolinite content ≥40%, provides dense microstructure giving high mechanical performance and resistance to chemical substances penetration [4]. Natural pozzolana is natural pyroclastic rocks composed of volcanic glass that is rich in silica or combination of silica and alumina [5–7]. At modest replacement levels, substituting Portland cement with SCMs generally results in lower early age strength, however as pozzolanic reaction is ongoing, late age strength development is achieved [6,8,9]. To overcome the decrement in the compressive strength at early age, alkali activators have been utilized. For instance, Na_2SO_4 has shown to improve early strength of composite cement containing slag by promoting alite hydration [10]. Similar findings were reported in [11,12], where alkali activators enhanced the early strength of synthetic alite mixes through accelerating alite hydration. However, alkali activators can negatively impact long term strength development [13].

Investigating the evolution of the complex microstructure and porosity of low clinker binders is essential for understanding their mechanical and durability performances [14]. Differentiating the porosity and water volume population in the low clinker hydrated paste is critical to explain mechanical performances including strength, shrinkage, and creep. In parallel, the durability performance depends on a clear understanding of water distribution within the matured paste hydrates and associated porosity, as these factors govern water transport properties. These properties are fundamental for assessing the service life measurement of concrete exposed to carbonation or chloride ingress, hints the resistance of concretes against corrosion is evaluated [15–18].

The hydration of composite cements consists of pozzolanic or latent hydraulic reactions of SCMs with portlandite (CH), which forms during

* Corresponding author at: Institute of Building Materials Research at RWTH Aachen University, Aachen 52062, Germany and Heidelberg Materials, Global Research & Development, Oberklamweg 2-4, Leimen 69181, Germany.
E-mail address: ayshayasernawwaf.anagreh@heidelbergmaterials.com (A. Anagreh).

https://doi.org/10.1016/j.cemconres.2026.108209
Received 11 January 2026; Received in revised form 22 February 2026; Accepted 10 March 2026
Available online 17 March 2026

cement hydration in the presence of water (H). These reactions take place within the aqueous pore spaces [19]. The main products of cement hydration in presence of limestone are calcium aluminosilicate hydrate (C-A-S-H), portlandite (CH), ettringite (AFt), and carboaluminate phases (AFm). Additionally, the pozzolanic reaction of amorphous alumina and silica (Al—Si) contributes to the formation of C-(A)-S-H gel and carboaluminate AFm ($C_3A.Cc.H_{11}$) phases, as described in stoichiometry Eq. (1). These phases play a crucial role in refining pore structure and enhancing mechanical strength [6,20,21].

$$\text{Al}\blacksquare\text{Si amorphous} + CH + H \rightarrow C-(A)-S-H + C_3A.Cc.H_{11} \quad (1)$$

The governing factors for continued hydration of low clinker pastes containing cement ≤50%, is the availability of CH, adequate pore space, and sufficient water [1,3,19,21–24]. In systems with higher clinker content, such as limestone calcined clay cement with 55% Portland cement, hydration at later ages progress slowly, even after 3 years, primarily due to the reduction in water filled capillary porosity [22,24]. The residual water remains on the pore surface could enable the continued growth of hydration products [19]. Nevertheless, for the mixtures with low clinker content <50%, the extent to which this reduction in water filled porosity influences ongoing hydration remains unclear.

Pores partially or fully filled with solution in the hydrated cement paste are categorizing based on the pore size as [22,23,25–27]: capillary with pore size range of 10 nm–100 μm, represent the bigger porosity spaces, not filled by solid phases, and partially or fully emptied from water, smallest of these pores called interhydrate water pores of approximately 10–100 nm, located between C-(A)-S-H gel needles. In addition, water filled pores incorporated in C-(A)-S-H gel is divided into gel water pores formed due to the agglomeration of C-(A)-S-H gel sheets presenting the spaces created by staking the sheets with size range between 1 and 10 nm and interlayer water located in C-(A)-S-H gel sheets as a part of its structure with pore size ≤1 nm [25–27].

Different experimental techniques were adopted in characterizing the porosity volume of the hydrated paste, such as mercury intrusion porosimetry (MIP), which is applied on dried samples to determine the volume of capillary and interhydrate pores by forcing the mercury penetration into the pore network under gradually increased pressure [4,23,28]. Although previous studies have reported certain limitations of the MIP technique, such as the ink bottle effect, which occurs when higher pressure is required for the mercury to intrude larger pores that are only accessible through narrow connected pathway [28,29], it has nonetheless been shown to accurately measure the capillary pore volume, a conclusion supported ^{1}H NMR results [23,29]. To categorize and quantify nanoscale pore populations, including heterogeneous C-(A)-S-H interlayer water and gel water, ^{1}H NMR relaxometry was applied [26,29]. However, ^{1}H NMR cannot detect the pores that have been emptied of water [30]. Also, this technique is sensitive to materials with high iron content, as it could disrupt the magnetic homogeneity [31]. Dynamic water vapor sorption (DVS) was also used to characterize the porosity in the hydrated paste, where it measures moisture change in the sample as a function of the relative humidity (RH) % [32–34]. This technique enables the penetration of fine pores through water sorption, since water molecules are smaller than other sorption gases, such as nitrogen [35,36]. Scanning electron microscopy (SEM) image analysis is applicable for detecting the chemical composition of the studied samples, C-(A)-S-H gel composition, morphology and the evolution of the microstructure [24,37]. However, it is proven not to be the right method to measure the fine porosity of less than one μm [23].

Applying these analytical methods alone does not fully reveal the mechanisms behind the microstructural development of low clinker binders. Alderete et al. [36] demonstrated that DVS and MIP techniques complement each other in evaluating pore connectivity and distribution across systems with cement replacement levels of up to 60% with ground-granulated blast-furnace slag at different ages. An integrated approach is required to correlate the amount of water within the pore structure, the complete pore size distribution, and the resulting hydrated microstructure in low clinker binders with different SCMs.

Understanding the role of the water availability and distribution within the microstructure of composite cements with low clinker content at different ages is important for characterizing the mechanisms behind the compressive strength performance. Therefore, in this study, different measurement techniques were combined to quantify the water content and distribution in the hydrated low clinker pastes with clinker content ≤45% mixed with either calcined clay or natural pozzolana in addition to limestone at different proportions. The investigation highlights the importance of the water mass balance method in first reflecting the pore volume and porosity distribution of low clinker binders and to use it as an input data to quantify C-(A)-S-H gel volume in the hydrated low clinker pastes. The water mass balance approach was validated by MIP, DVS, volume balance, bound water calculated by thermogravimetric analysis (TGA), and drying at 40 °C then at 600 °C. In addition, the consistency of different measurement methods used to quantify the water mass distribution in low clinker binder pastes was evaluated.

2. Materials and methods

2.1. Raw materials

A commercial CEM I 52.5 R cement according to EN 197-1 and a limestone powder with $CaCO_3$ content of 95.7% measured by thermogravimetric analysis (TGA) were used in this study. The SCMs studied were calcined clay (CC) with calcined kaolinite content of 47.8%, and natural pozzolana (NP).

The natural pozzolana is contaminated with around 7% of clinker due to the industrial production process, which has been considered in the mixture designs containing natural pozzolana. The CEM I content was adjusted down considering the 7% clinker coming with the natural pozzolan.

To optimize the sulfate content in the studied systems, an external sulfate source was incorporated. Hemihydrate was used in calcined clay mixtures, whereas calcium sulfate (gypsum) was used in natural pozzolana mixtures.

The materials chemical and mineralogical compositions characterized by X-ray fluorescence (XRF) and Rietveld quantitative X-ray powder diffraction (QXRD) are shown in Table 1. Particle size distributions percentiles, distribution spans and specific surface area measured using nitrogen adsorption method (BET) of all constituents are presented in Table 2.

2.2. Composite cement mixture design

Different proportions of either calcined clay or natural pozzolana combined with cement content ≤45% and limestone were studied to assess the effect of low clinker binders on the evolution of phase assemblage, water distribution and porosity within these hydrated systems. The mixture designs are presented in Table 3.

The reference systems contained either 45% or 35% of CEM I with 55% or 65% limestone on a mass basis with an additional amount of hemihydrate to achieve a uniform sulfate level of 3.2% SO_3 among all systems, acknowledging that natural pozzolana systems generally require less sulfate than calcined kaolinitic clay due to their lower reactive aluminium content.

The addition of calcined clay and natural pozzolana was on mass basis in groups of 20%, 45%, and 45% + sodium sulfate (N$), with actual SCM proportions (detailed in Table 3) varying according to clinker content in both binder groups of 45% and 35%. This design aimed to investigate the impact of increasing SCM content from zero to 20% then to around 45% on the hydration mechanisms of low-clinker systems, moving beyond the extensively studied composite binders with a 2:1 calcined clay-to-limestone ratio.

Table 1
LOI (loss on ignition), chemical compositions (XRF) and main phase compositions (QXRD) of the starting materials (wt%).

Raw materials	Cem I 52.5 R	Calcined clay	Natural pozzolana	Limestone	Hemihydrate	Gypsum
LOI	1.32	2.36	0.38	42.13	7.85	21.20
SiO_2	20.89	60.25	44.44	1.98	0.72	0.95
Al_2O_3	5.53	25.80	12.73	0.53	0.02	0.33
Fe_2O_3	2.04	8.87	11.06	0.30	0.02	0.15
CaO	63.85	0.98	17.75	54.16	38.67	32.22
Na_2O	0.03	–	1.63	–	–	0.03
K_2O	0.83	0.17	0.39	0.08	0.01	0.04
MnO	0.04	–	0.18	0.05	–	–
TiO_2	0.29	1.26	1.40	0.04	–	0.02
MgO	1.70	0.24	9.50	0.61	0.07	0.17
P_2O_5	0.12	0.02	0.16	0.01	–	0.03
SO_3	3.36	0.05	0.39	0.11	52.63	44.86
Alite	58.30	–	5.29	–	–	–
Belite	15.60	–	3.39	–	–	–
$C_3A + C_4AF$	17.10	–	2.20	–	–	–
Anhydrite	1.10	–	–	–	–	–
Portlandite	0.40	–	–	–	–	–
Quartz	0.50	27.40	–	0.90	–	–
Calcite	1.60	1.00	1.40	95.9	–	–
Others	5.40	8.80	31.54	3.20	–	–
Amorphous content	–	62.80	56.19	–	–	–

Table 2
Particle size distributions, specific surface area, and densities of the raw materials.

Raw materials	CEM I 52.5 R	Calcined clay	Natural pozzolana	Limestone	Hemihydrate	Gypsum
$Dv_{,10}$ (μm)	1.20	2.34	1.15	1.33	2.53	6.84
$Dv_{,50}$ (μm)	8.25	16.30	5.22	9.85	21.50	26.40
$Dv_{,90}$ (μm)	26.60	52.00	17.50	77.90	58.60	47.00
Span (−)	3.08	3.05	3.13	7.77	2.60	1.52
BET (m^2/g)	1.98	47.16	2.30	1.50	–	–
Density (g/cm^3)	3.13	2.74	2.93	2.75	2.76	2.34

Table 3
Mixture proportions of the low clinker systems investigated (wt%).

Binder label	Cem I 52.5 R	Calcined clay	Natural pozzolana	Limestone	Hemihydrate	Gypsum	Sodium sulfate
C45.L55	45.00	–	–	51.80	3.20	–	–
C45.CC20.L35	45.00	18.80	–	33.00	3.20	–	–
C45.CC45.L10	45.00	42.30	–	9.50	3.20	–	–
C45.CC45.L10 + 1.5 N$	45.00	42.30	–	11.10	1.60	–	1.50
C45.NP20.L35	43.50	–	20.20	32.40	–	3.80	–
C45.NP45.L10	41.60	–	45.50	8.90	–	3.80	–
C45.NP45.L10 + 1.5 N$	41.60	–	45.50	10.80	–	1.90	1.50
C35.L65	35.00	–	–	61.10	3.90	–	–
C35.CC20.L45	35.00	18.80	–	42.30	3.90	–	–
C35.CC45.L20	35.00	42.30	–	18.80	3.90	–	–
C35.CC45.L20 + 1.5 N$	35.00	42.30	–	20.50	2.20	–	1.50
C35.NP20.L45	33.50	–	20.20	41.70	–	4.50	–
C35.NP45.L20	31.60	–	45.50	18.20	–	4.50	–
C35.NP45.L20 + 1.5 N$	31.60	–	45.50	20.00	–	2.60	1.50

A fixed water-to-binder (w/b) ratio of 0.5 was used for all pastes and mortars. A sodium sulfate (N$) dosage of 1.5% of the dry mass of the binder was added to the mixtures containing the highest SCM content, to evaluate the impact of alkali on these systems. To enhance the workability of the calcined clay mortars and achieve consistency of the mixes with natural pozzolana and limestone, polycarboxylate ether superplasticizer of maximum 1.02% of dry mass was added.

The mixtures were named as CX.CC/NPY.LZ, where X indicates cement content of either 45% (corresponding to 45%, 43.5%, and 41.6%), or 35% (including 35%, 33.5%, and 31.6%), Y refers to the SCM content of 20% (18.8% and 20.2%), or 45% (42.3% and 45.5%), and Z to the amount of limestone added as presented in Table 3. Gypsum and hemihydrate contents differ due to their SO_3 contents, as seen in Table 1.

2.3. Portlandite blend

Synthetic portlandite pastes were prepared by mixing portlandite with calcined clay and limestone, maintaining a portlandite to calcined clay ratio of 3:1, to avoid complete portlandite consumption. In addition, sodium hydroxide was pre-dissolved in the mixing water and then combined with the dry mix to better simulate the alkaline environment of cement pore solutions [38]. Table 4 summarizes the composition portlandite paste.

Table 4
Composition of synthetic portlandite mixture (wt%).

Mixture	Portlandite (CH)	Calcined clay (CC)	Limestone (L)	NaOH
CH_CC_L	66.8	22.3	10	1

2.4. Experimental study

2.4.1. Hydration and porosity studies on paste

Pastes were prepared by mixing approximately 100 g of dry powder with 50 g of distilled water using a vertical axis high shear mixer at 1400 rpm for 3 min. The resulting paste was transferred into cylindrical plastic moulds with dimensions of 3.2 cm × 6.8 cm, closed with a lid and sealed with parafilm. The samples were cured at room temperature (20 ± 1 °C) until testing. Hydration studies were conducted at 7, 28 and 90 days after casting.

QXRD was performed on freshly cut specimens to evaluate the phase assemblage changes resulting from different proportions of SCMs and curing ages. A disk of 3–4 mm was cut from the sample and placed into the XRD sample holder for analysis. Bruker ENDOVER in θ-2θ configuration with divergence opening of 0.14° was used. Samples were scanned between 4 and 72° (2θ) with a step size of 0.019°, a time step of 0.4 s, and a total scan duration of approximately 20 min. All samples had XRD refined with Rietveld analysis using TOPAS 6.0 (Bruker AXS, Karlsruhe, Germany) software [39]. The external standard method was used for the amorphous phase quantification. A high purity quartz reference (≈100% purity) was measured separately under identical instrumental conditions to determine the instrument specific constant (k-factor). The k-factor was calculated from the refined scale factor, density, unit cell volume, weight fraction (≈1 for pure quartz), and the mass attenuation coefficient of the quartz standard. This calibration was repeated at the beginning of each measurement day to account for potential instrumental drift, ensuring reliable and consistent amorphous content determination. The associated uncertainty of the method is approximately ±2%.

The solvent exchange drying method employed in this study was carried out on 15 g of hydrated paste powders. To stop the hydration, the powders were first immerged in isopropanol (purity >95%) for 10 min and vacuum filtered, followed by 10 min immersion in petroleum ether to remove residual isopropanol, and again vacuum filtered. The treated powders were then stored in a desiccator for at least 48 h to ensure complete evaporation of the petroleum ether. Subsequently, the dried samples were ground to a particle size of ≤63 μm for thermogravimetric analysis (TGA).

Thermogravimetric analysis (TGA) was done on the dried grounded pastes (< 63 μm). Around 20–30 mg of the powder of around was placed in 85 μL alumina crucible and inserted in the instrument NETZSCH TG 209F1 Libra. The temperature started from 30 °C and kept increasing at rate 10 °C/min till reaching around 950 °C under N_2.

Mercury intrusion porosimetry (MIP) was conducted to evaluate the capillary porosity of the hydrated low clinker pastes. After reaching the designated hydration age, the pastes were crushed into particles sized between 1 mm and 2 mm and dried using solvent exchange method. MIP measurements were conducted with a maximum intrusion pressure of 400 MPa and the analysis assumed a mercury contact angle of 140°.

Dynamic vapor sorption (DVS) Endeavour equipment from Surface Measurement Systems was performed on freshly crushed pastes at 20 °C to obtain the desorption curves that correlate water loss from gel and interlayer water with the relative humidity (RH). The controlled RH in the DVS was initially set at 98% and then decreased stepwise down to 5%. Following, sorption curve was conducted by increasing RH from 5% stepwise to 60%, then again, a desorption step was done by reducing the RH from 60% to 5%. Each RH step lasted approximately 440 min to change to the next RH, except for the initial step from 98% to 95%, which required 1440 min.

The mass changes detected in the DVS desorption curves were normalized by taking the sample from DVS to the TGA technique, to determine the binder dry mass at 600 °C, at which both free and bound water are fully released, while the water associated with calcium sulfates and CO_2 from calcium carbonate, remain within the systems. The measurement uncertainty was estimated to be ≤ 0.04 g/100 g, based on the standard deviation of the normalized DVS mass obtained from repeated measurements of one mixture at 28 days. Kelvin Laplace Eq. (2) was applied to calculate the maximum pore size occupied with water thus enabling the distinction between gel water and interlayer water in their desorption profiles. The water loss between 31% - 5% RH was considered as interlayer water with targeted pore size <1 nm, while gel water was calculated based on the water loss between 90% - 35% RH with 1 nm < pore size ≤10 nm.

$$\ln\left(\frac{P}{P0}\right) = \ln(\mathrm{RHk}) = \frac{2\gamma Vw}{rRT} \quad (2)$$

P (Pa) and P0 (Pa) are vapor pressure and saturated vapor pressure, respectively. Vw is the molar volume of the water which is 1.8×10^{-5} m^3/mol, γ of 0.07286 N/m is the interfacial energy of pure water (without dissolved salts), $R = 8.314$ J/kMol is the universal gas constant and r (m) is the pore radius to be calculated. All values are at temperature 293.15 K (20 °C) [22].

Chemical shrinkage was applied to calculate the volume of the empty pores that are formed due to the self-desiccation. Pastes of 9.0 ± 0.8 g with the mix designs mentioned in Table 3 were filled with distilled water on top without diluting the cement paste, to allow the samples while hydrating to suck the above water to balance the effect of the chemical shrinkage [40]. Levelled pipettes were filled with coloured oil and placed above the water filled pastes to show the change of the water level. In addition, 5 duplicates of each mix design were conducted and 4 references of water with pipettes filed with oil were applied [23]. Measurements were recorded three times daily during the first week, twice daily in the second week, once daily in the third week, and subsequently reduced to once or twice per week.

The R^3 heat release test was conducted on calcined kaolinitic clay and natural pozzolana materials to evaluate their reactivity, following the ASTM C1897/EN 196-12 isothermal calorimetry method.

The volume balance approach (cm^3/g) of hydrated pastes at 7 and 90 days was determined as follows:

1. The mass of the crystalline phases including anhydrous clinker phases, crystalline hydrates (AFt, AFm as the sum of hemicarboaluminate and monocarboaluminate, and CH), as well as SCMs inert were quantified using XRD Rietveld analysis.
2. Fe_2O_3 remaining from clinker and SCMs crystalline inert phases is assumed to be incorporated into siliceous Fe-hydrogarnet with composition $C_3FS_{0.84}H_{4.32}$ [41].
3. The hydrates masses were converted to their corresponding volumes, using density values taken from [42–44], which are presented in Table 5.
4. C-(A)-S-H gel layer volume is calculated based on the interlayer water mass (obtained from DVS). The ratio of interlayer water mass

Table 5
Densities of the crystalline phases.

Crystalline phases	Density g/cm^3
AFt [42]	1.778
Hemicarboaluminate (Hc) [42]	1.985
Monocarboaluminate (Mc) [42]	2.175
CH [42]	2.251
C_2S-beta [42]	3.326
C_4AF [42]	3.708
$CaCO_3$ [42]	2.710
Dolomite [42]	2.852
Quartz [42]	2.641
Fe-Hydrogarnet [42]	2.809
Periclase [42]	3.584
Forsterite-iron [43]	3.320
Andesine [44]	2.660
Anatase [44]	3,890
Diopside [44]	3.300
Hematite [44]	5.260

to C-(A)-S-H gel solid layer volume is 0.46, excluding gel pore water, as reported by Muller [45] using ^{1}H NMR data.

5. The initial paste volume was calculated by summing the ratios of each component mass (wt% values mentioned in Table 3 of the 100 g total dry mix) to its respective density in the mixture design. The corresponding component densities applied in this calculation are listed in Table 2.
6. The volume of unreacted SCMs and amorphous components (including siliceous Fe-hydrogarnet) is defined as the difference between the initial paste volume and the combined volumes of the crystalline phases, the C-(A)-S-H gel sheet layers, the gel pores, and both saturated and empty capillary pores.

2.4.2. Compressive strength test on mortars

Compressive strength was conducted on all mix designs listed in Table 3 according to the European standard EN 196. The compressive strength was measured after 7 and 90 days.

3. Results

3.1. Capillary porosity

To evaluate the capillary porosity distribution within the hydrated pastes, MIP technique was applied. Fig. 1 presents the MIP curves for binder groups 35% and 45% at 7 days, illustrating the changes in the critical pore entry diameter among reference, natural pozzolana and calcined clay systems. The reference mixes show the largest critical pore entry diameters. Upon the addition of either calcined clay or natural pozzolana, the peak shifts toward smaller pore sizes, with calcined clay mixtures exhibiting the smallest pore entry diameters. As seen in Fig. 1, both C45.CC45.L10 and C35.CC45.L20 mixtures are reflected in two distinct populations of connected porosity. The first peak is comparable to that of mixtures with 20% calcined clay, indicating similar pore population and overall porosity. The second peak corresponds to a finer connected pore population compared to both 20% calcined clay and limestone reference mixes.

Fig. 2 illustrate the MIP curves at 90 days for reference mixes, as well as those incorporating either calcined clay or natural pozzolana, for both binder groups of 35% and 45%. The critical pore entry diameter corresponding to the coarse pore population observed at 7 days (Fig. 1) in C35.NP45.L20 and C45.NP45.L10 mixtures significantly decreased at 90 days, indicating progressive microstructural refinement. In general, the addition of natural pozzolana consistently shifted the critical pore entry diameter toward a finer pore size distribution. According to Fig. 2, the C35.CC45.L20 mixture exhibits both coarse and pore populations, suggesting the presence of capillary pores, interhydrate pores, and very fine pore fraction [23]. In contrast, the C45.CC45.L10 mixture demonstrates only very fine pore population.

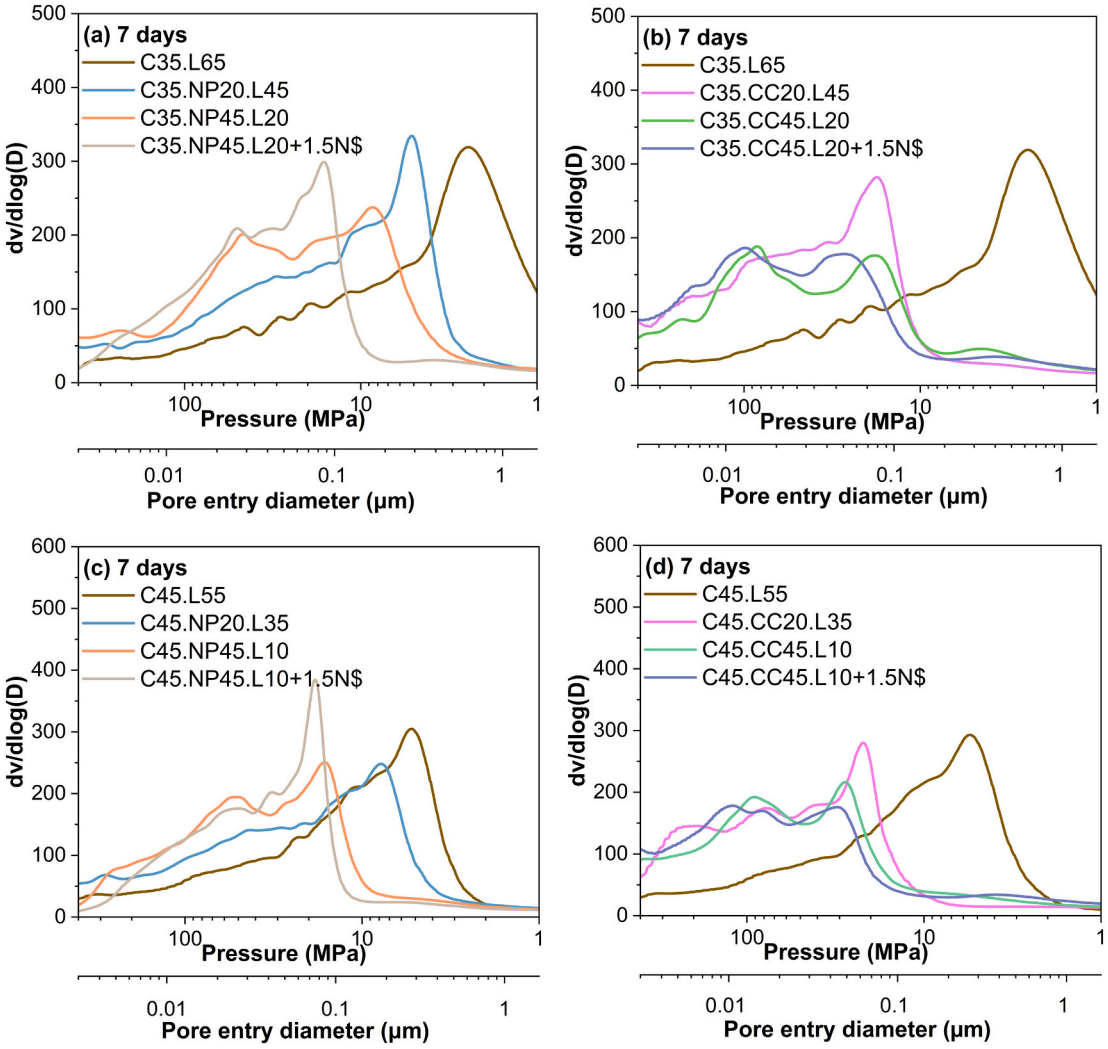

Fig. 1. MIP curves after 7 days of curing for (a) 35% binder mixtures with reference and natural pozzolana, (b) 35% binder mixtures with reference and calcined clay, (c) 45% binder mixtures with reference and natural pozzolana, and (d) 45% binder mixtures with reference and calcined clay.

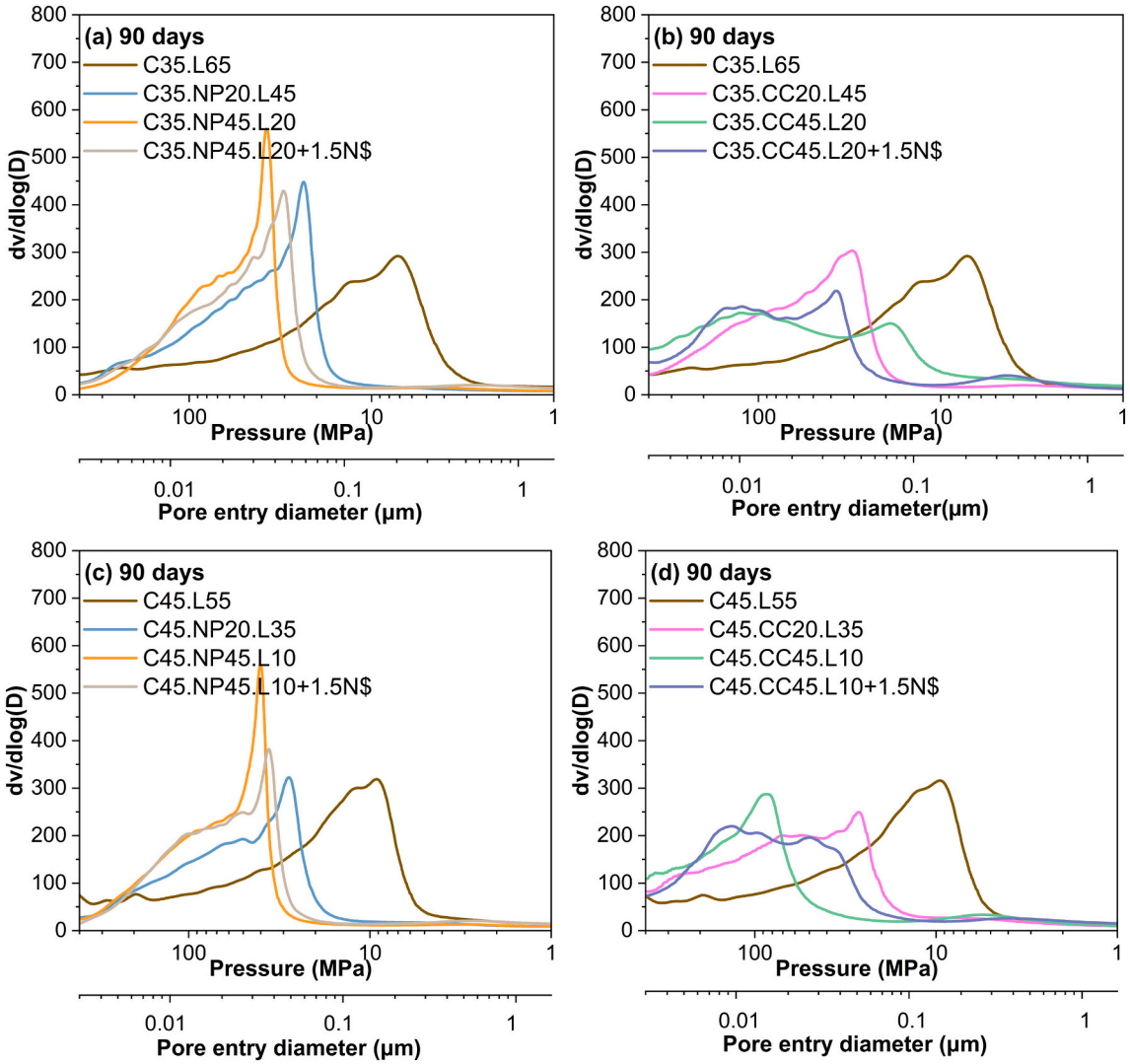

Fig. 2. MIP curves after 90 days of curing for (a) 35% binder mixtures with reference and natural pozzolana, (b) 35% binder mixtures with reference and calcined clay, (c) 45% binder mixtures with reference and natural pozzolana, and (d) 45% binder mixtures with reference and calcined clay.

As observed in Fig. 1, the alkali activated natural pozzolana mixtures for both binder groups at 7 days exhibited the smallest critical pore entry diameters, this reduction in the porosity is due to the early age enhancement of the hydration induced by the addition of sodium sulfate [46]. However, at later age the peak shifts behind the mixture with 45% natural pozzolana, suggesting reduced hydrate precipitation due to the desaturation of larger pores, as reported in [13].

Consistent with previous studies [28,47,48], the MIP measurements performed in this study successfully captured microstructural changes in the hydrated pastes at 7 and 90 days by identifying variations in the critical pore entry diameter, as illustrated in Fig. 1 and Fig. 2.

3.2. Fine pore structure

To characterize the changes in water filled fine pores within the hydrated pastes of binder groups (35% and 45%) containing reference, calcined clay, and natural pozzolana at 7 and 90 days, dynamic vapor sorption (DVS) technique was conducted. Desorption curves were generated, capturing the changes in sample mass as a function of relative humidity (RH) %, where RH step was changing based on the change of the mass over specific time interval.

Fig. 3 shows the desorption profiles of both binder groups 35% and 45% at 7 days. Mixes containing calcined clay exhibit greater water retention within the fine pore region ($\leq$ 10 nm) in comparison to the natural pozzolana and the limestone reference systems, suggesting accelerated formation of C-(A)-S-H gel phases. Fig. 4 presents the desorption profiles of both binder groups 35% and 45% at 90 days. At this extended curing age, water retention in natural pozzolana mixes have increased and became equivalent to those observed in the calcined clay mixes for both binder groups. This observation indicates that natural pozzolana systems have faced further pozzolanic reaction at a later age, suggesting the formation of comparable levels of C-(A)-S-H gel to those in the calcined clay systems. At 90 days, the highest water retention corresponding to pores $\leq$1 nm was observed in mixtures with the highest proportions of either natural pozzolana or calcined clay. While reference systems show the lowest water retention at both ages 7 and 90 days as observed in Fig. 3 and Fig. 4. As expected, mixtures with higher clinker contents show higher water retention compared to those with 35%.

The impact of sodium sulfate addition on fine pore characteristics of the binders is reflected in the desorption curves. At both 7 and 90 days, the mixtures with 45% calcined clay activated with sodium sulfate exhibit lower water retention in the desorption curves for pores around 1 nm compared to the same mixtures without activation. However, the desorption curve at 7 days for the natural pozzolana and sodium sulfate mixtures indicate equal or greater water retention compared to the same

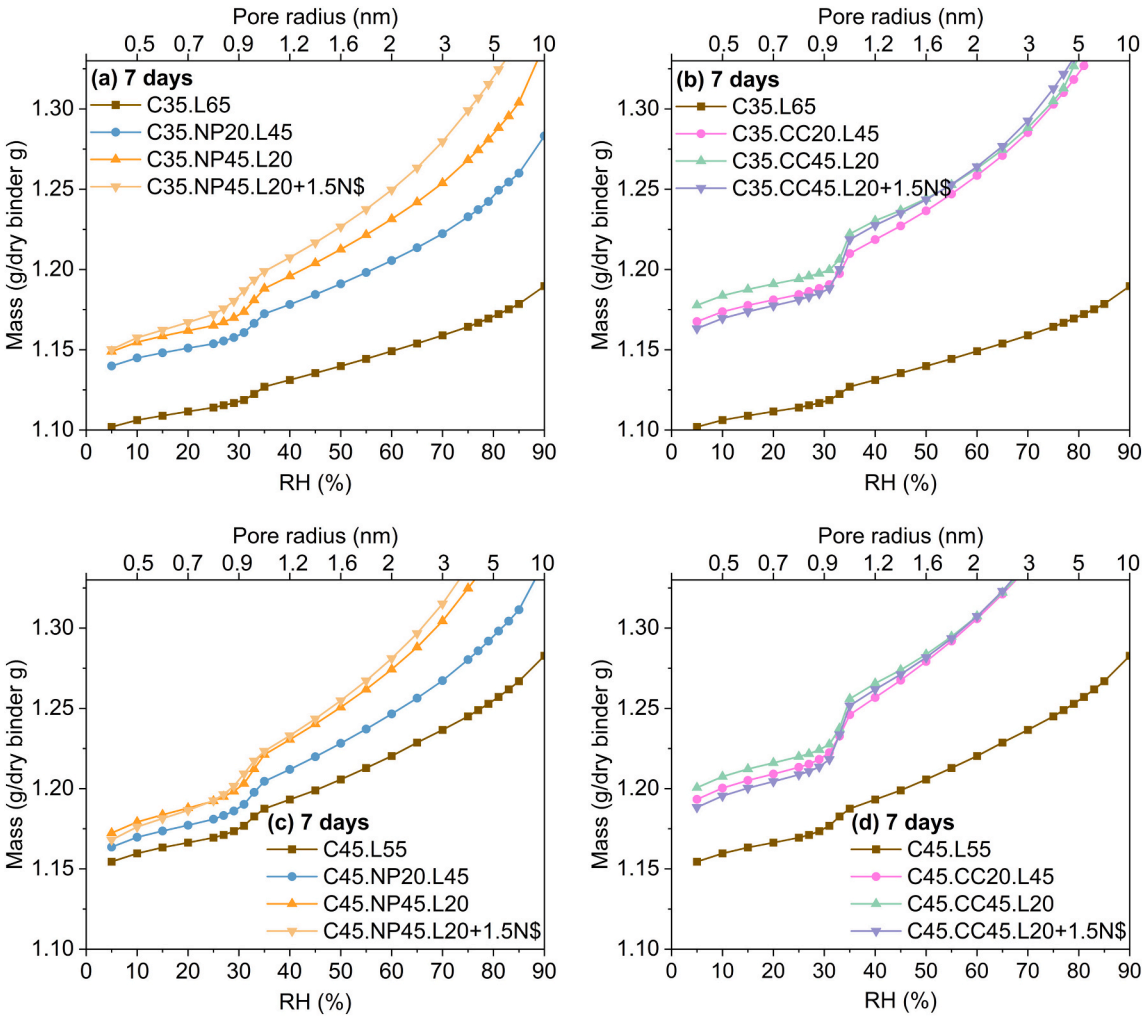

Fig. 3. Desorption curves at 7 days for hydrated pastes of binder mixtures: (a) 35% reference and natural pozzolana, (b) 35% reference and calcined clay, (c) 45% reference and natural pozzolana, and (d) 45% reference and calcined clay.

mixtures without sodium sulfate. These observations confirm that the addition of sodium sulfate boosts the early age hydration promoting C-(A)-S-H gel formation, but adversely affects the hydration at later stages [13]. In calcined clay systems, this negative impact appears as early as 7 days due to their rapid reactivity and faster consumption of the saturated spaces, while in natural pozzolana systems, it becomes evident only beyond 7 days.

Additionally, DVS measurement was conducted on calcined clay and natural pozzolan materials to evaluate the fine pores within these materials. Fig. 5 illustrates the mass change of the starting materials as a function of RH%. The mass of natural pozzolana remains unchanged with varying RH%. On the other hand, calcined clay demonstrates a clear desorption profile with mass decrement as RH% drops, indicating the presence of fine pores $\leq$10 nm. This observation aligns with Ferrari et al. study [49], who identified the presence of internal pores in calcined clay of size below 40 nm, reaching down to 6 nm using differential scanning calorimetry (DSC) and 16-time domain nuclear magnetic resonance (^{1}H TD-NMR).

A detailed interpretation of the desorption curves of the low clinker mixtures with either natural pozzolana or calcined clay is challenging due to the complexity of the hydrated pastes microstructure and the heterogeneous of calcined clay and natural pozzolana materials. Therefore, further investigations of the water incorporated with C-(A)-S-H gel in low clinker systems are required using other techniques, such as ^{1}H NMR.

3.3. Water mass distribution

As reported in previous studies [6,21,23,24], continued hydration requires the presence of water filled pores with the sufficient size. To better explain the mechanical performance and provide a comprehensive characterization of hydrate formation, porosity reduction, and water distribution within the pore network in low clinker pastes over time, a novel water mass balance is introduced, unlocking a deeper understanding of the hydration phenomena. Water mass balance was conducted by integrating various analytical techniques, as detailed in the following sections.

3.3.1. Crystalline water

The chemically bound water within each crystalline phase, as identified by QXRD, was quantified by first calculating the masses of CH, AFt, and AFm, and normalizing them to the anhydrous binder mass. The normalized values were subsequently multiplied by ratio of the molar mass of water in the phase to the molar mass of the respective phase. The results were expressed as the equivalent water content in grams per gram of binder. Fig. 6 presents the crystalline water content of the reference, natural pozzolana and calcined clay mixtures at ages 7, 28 and 90 days, corresponding to the binder mixtures 35% and 45%.

According to QXRD results, the water content associated with ettringite (AFt) showed minimal variation over time among the systems, due to the similar SO_3 content in these mixes. This observation is

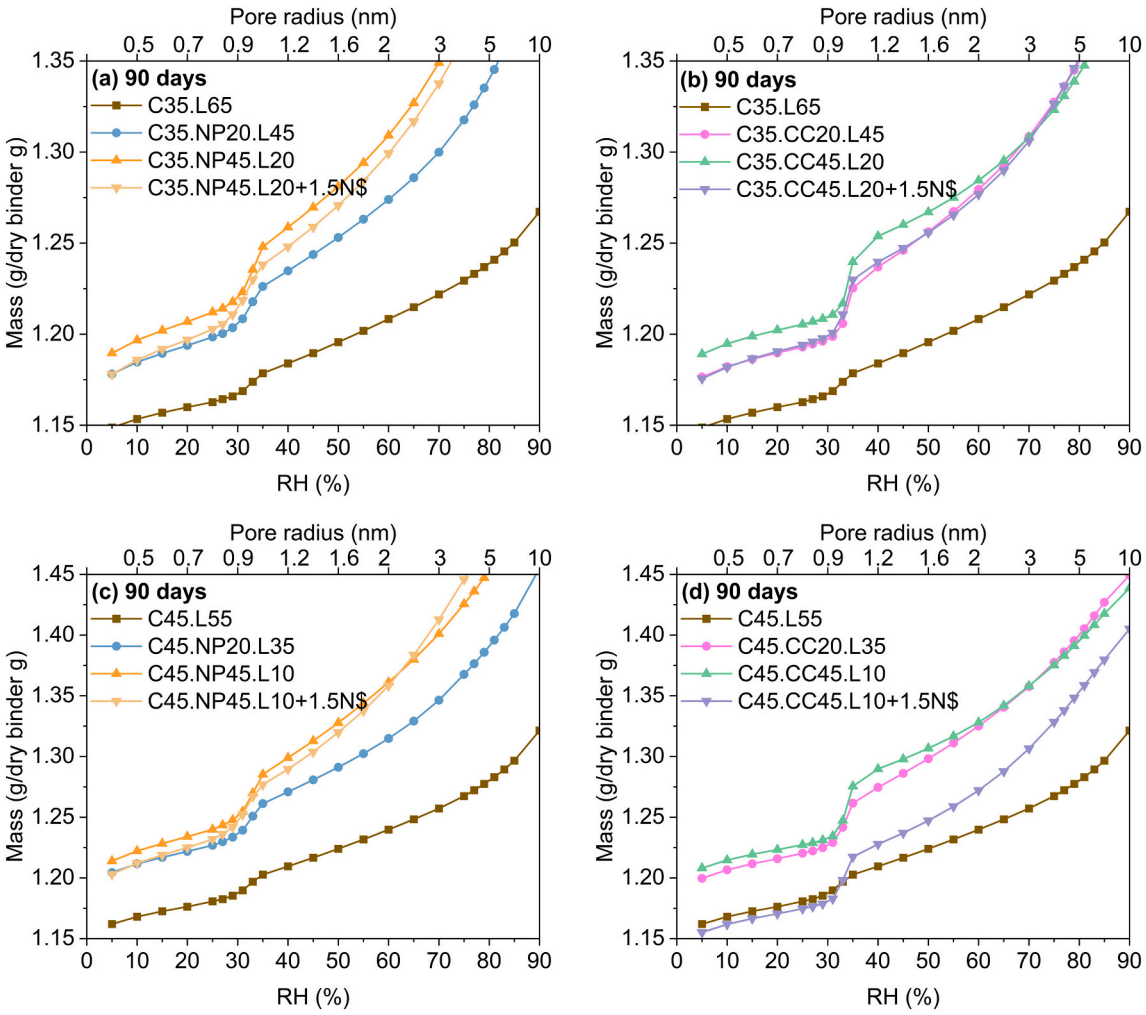

Fig. 4. Desorption curves at 90 days for hydrated pastes of binder mixtures: (a) 35% reference and natural pozzolana, (b) 35% reference and calcined clay, (c) 45% reference and natural pozzolana, and (d) 45% reference and calcined clay.

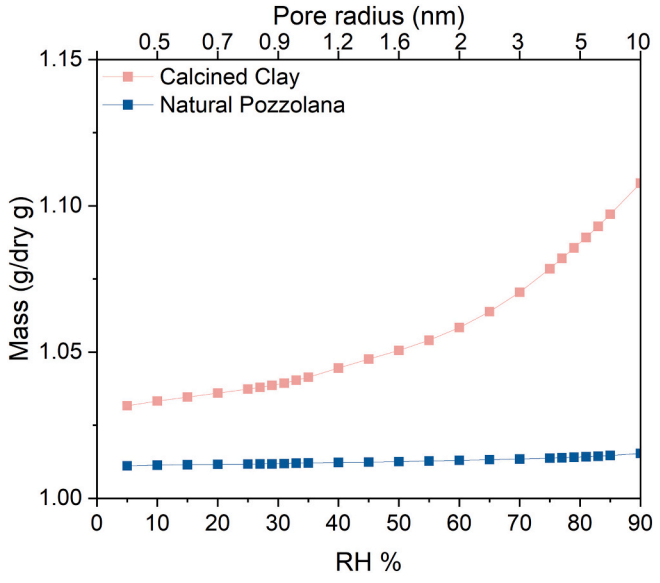

Fig. 5. Desorption profiles of the studied SCMs.

consistent with the findings in [21,24]. The water amount linked to AFm phases showed a considerable reduction with higher calcined clay content in the mixes with higher clinker level at 90 days. This phenomena was explained in [4], attributing it to the calcined clay high reactivity, which accelerates the filling of the saturated capillary pores that are larger than the critical pore size required for AFm growth. A minor increment in AFm water content of up to approximately ±1.2% is observed in natural pozzolana systems, this variation remains within the XRD estimated measurement uncertainty. Meanwhile, the water content of AFm phases increases with the addition of either calcined clay or natural pozzolana in comparison to the reference systems, indicating that aluminates from these materials is contributing with C_3A and C_4AF to AFm formation [21].

In natural pozzolana mixes, CH gradually decreases as the pozzolanic reaction progresses, whereas in calcined clay mixes, CH is fully consumed within 7 days.

3.3.2. *Water within the C-(A)-S-H gel*

To quantify the interlayer and gel water associated with the C-(A)-S-H gel in the hydrated paste samples at curing age of 7, 28, and 90 days, DVS desorption curves were obtained.

The DVS desorption profiles shown in Fig. 3 and Fig. 4, indicate a pronounced decrease in water mass between 35% and 31% RH. This drop is attributed to homogeneous cavitation occurrence within the gel

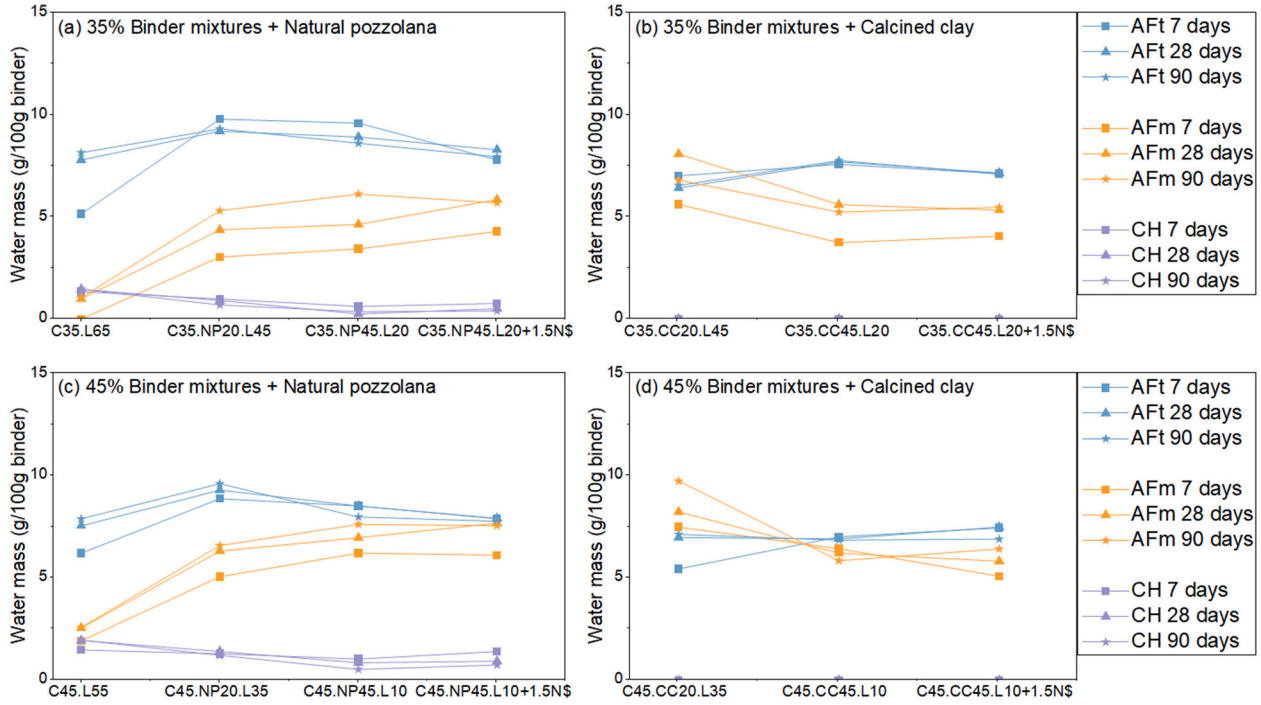

Fig. 6. Crystalline water distribution (measurement uncertainty ±2%) at 7, 28, and 90 days for (a) 35% binder mixtures of reference and natural pozzolana, (b) 35% binder mixtures with calcined clay, (c) 45% binder mixtures of reference and natural pozzolana, and (d) 45% binder mixtures with calcined clay.

pores restricted by the narrow interlayer spaces of the C-(A)-S-H gel, and is triggered by the development of negative pressure as the RH approaches approximately 30% [27,32]. Because this mass loss results from cavitation rather than true gel water release, the mass loss detected between 35% and 31% RH is excluded from the calculation of water incorporated in the C-(A)-S-H gel phases.

Fig. 7 and Fig. 8 present the calculated water distribution, including the water associated with C-(A)-S-H gel phases, crystalline water, and residual water in capillary pores within hydrated binder mixtures of reference, natural pozzolana and calcined clay for binder groups 35% and 45%, respectively.

It is observed that gel water content in natural pozzolana mixtures of both binder mixture groups is increasing between 7 and 28 days, which is further enhanced with the higher natural pozzolana content in the mixture. Furthermore, interlayer water slightly increases with the addition of natural pozzolana mixtures particularly between 7 and 90

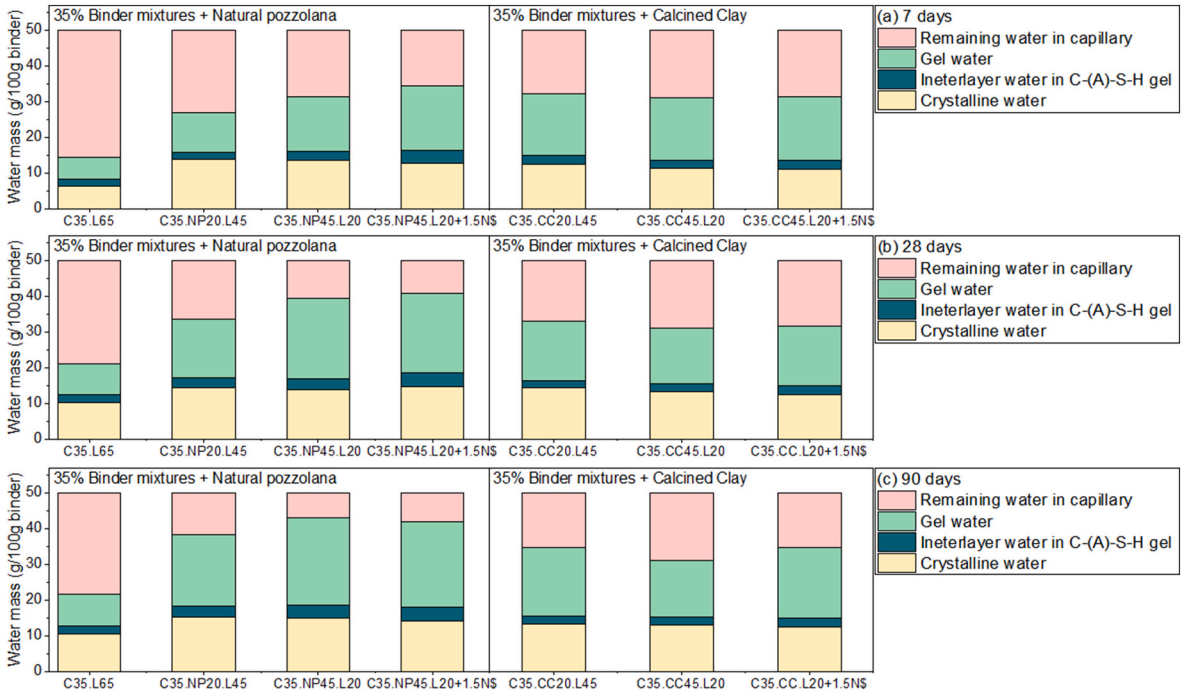

Fig. 7. Water mass distribution of 35% binder mixtures with natural pozzolana and calcined clay at (a) 7 days, (b) 28 days, and (c) 90 days (The maximum overall measurement uncertainty is approximately ≈ ± 0.22 g/100 g).

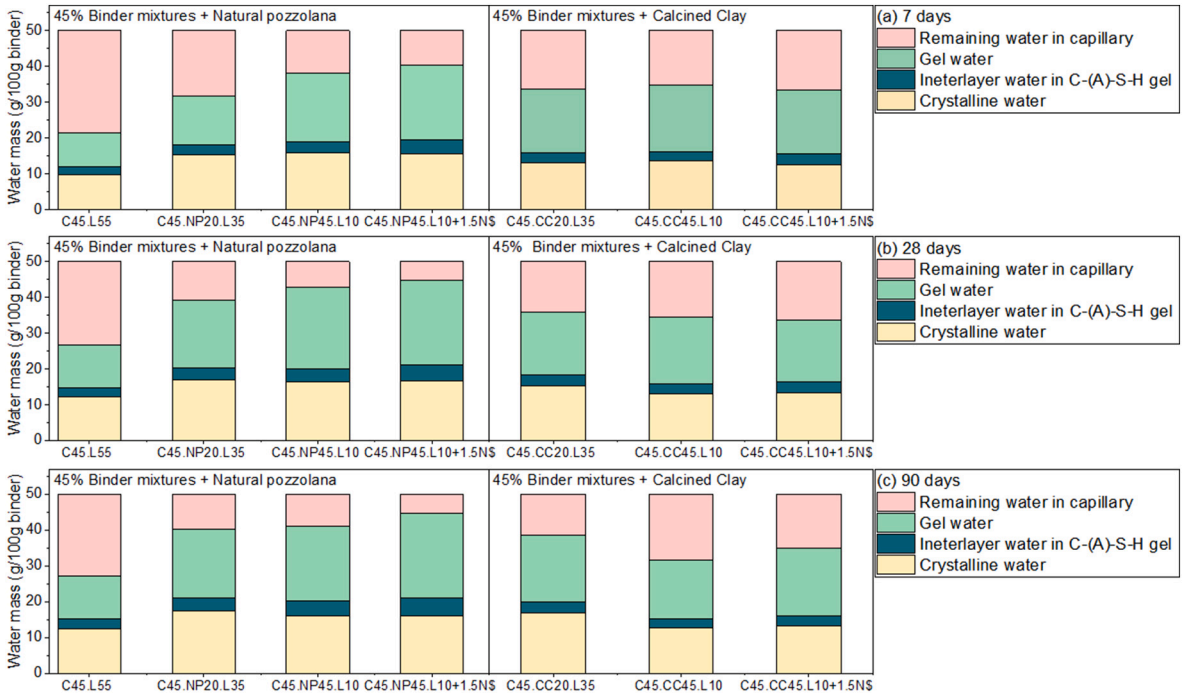

Fig. 8. Water mass distribution of 45% binder mixtures with natural pozzolana and calcined clay at (a) 7 days, (b) 28 days, and (c) 90 days (The maximum overall measurement uncertainty is approximately ≈ ± 0.24 g/100 g).

days, enhancing the formation of C-(A)-S-H gel content during this interval [4].

In case of calcined clay mixes, as shown in Fig. 7 and Fig. 8, interlayer water is not varying with calcined clay content between 20% and 45% irrespective of the cement content. The hypothesis behind this behavior is the presence of a fine internal pore structure in the calcined clay material below 10 nm, as seen in Fig. 5, contributing to the water content included in the C-(A)-S-H gel determined by DVS. The interpretation of this hypothesis is discussed in the following Section 3.3.3. Gel water of calcined clay mixes at 7 and 28 days are similar for both 35% and 45% binder groups, however gel water at 90 days is significantly higher for 20% calcined clay mix in comparison to the mix of 45% calcined clay amount. Gel water content difference is minimal between the mix of 20% calcined clay and the mix of 45% calcined clay with sodium sulfate at 7, 28 and 90 days.

3.3.3. *Water retention in calcined clay structure*

As presented in Fig. 7 and Fig. 8, the amount of interlayer water in the calcined clay mixtures remains nearly constant. To verify the proposed hypothesis regarding the effect of calcined clay fine pores on interlayer water mass calculations, synthetic pastes of portlandite mixed with calcined clay along with limestone were prepared to assess the pozzolanic reaction of the calcined clay and quantify water retention within the unreacted amorphous pore structure.

The pozzolanic reaction between amorphous alumina and silica in metakaolin, portlandite and limestone leads to the formation of C-(A)-S-H gel and AFm phases, as illustrated by the stoichiometry Eq. (1) [50]. To estimate the mass of the reacted metakaolin (g/100 g), CH consumption at 28 days of 25.47 g/dry g was calculated by subtracting the initial mass provided in Table 4, from the normalized final mass, detected by TGA analysis. Subsequently, the molar ratio between metakaolin and CH consumption was determined. This calculation assumes a C-(A)-S-H gel atomic ratio of (Ca/Si = 1.5 and Al/Si = 0.15), based on SEM-EDX point analysis of composite cement containing 50% metakaolin, comparable to the content used in this study, with residual CH at 28 days [4], and considers all amorphous silica in calcined clay is incorporated in C-(A)-S-H gel formation.

Based on this approach, the degree of reaction (DoR) of metakaolin at 28 days was calculated to be 80.5%, according to Eq. (3) [41]. This outcome is consistent with the known behavior of calcined clay containing high calcined kaolinite and amorphous aluminate contents, which exhibits high reactivity [6,51].

$$DoR\ of\ metakaolin = \frac{(initial\ metakaolin\ mass - final\ metakaolin\ mass)\,x100}{initial\ metakaolin\ mass} \quad (3)$$

Applying the DoR of metakaolin at 28 days, along with the initial mass of calcined clay in the hydrated low clinker paste of C35.CC45.L20, and its amorphous content determined by QXRD, the amount of water held within the pores ≤10 nm in the unreacted amorphous calcined clay can be estimated from the desorption curve presented in Fig. 5. This

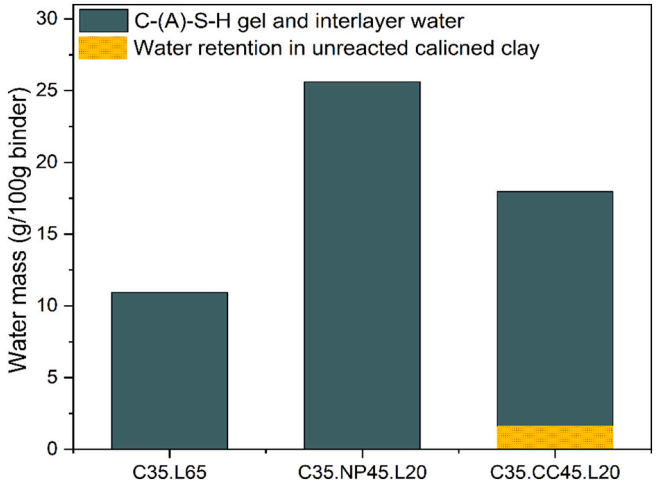

Fig. 9. Water mass associated with C-(A)-S-H gel in 35% binder mixtures of reference, natural pozzolana, and calcined clay at 28 days, along with water retained in the amorphous unreacted calcined clay within pore size ≤10 nm (measurement uncertainty of approximately ≤ 0.04 g/100 g).

estimation follows the same approach described in the methodology section, where water associated in C-(A)-S-H gel is determined using DVS desorption data, assuming all water in the clay resides in the amorphous phase.

Fig. 9 presents the calculated C-(A)-S-H gel and interlayer water in 35% binder mixtures of reference, natural pozzolana, and calcined clay systems, together with the estimated water content retained in the amorphous unreacted calcined clay pores (≤10 nm), which is around 1.6 g/dry mass. This comparison highlights that calcined clay can store water in pores similar in size to those of the C-(A)-S-H gel, however the stored amount is minimal, and thus its contribution to the DVS measured water content is not significant enough to affect the calculated C-(A)-S-H gel and interlayer water, considering the estimated DVS measurement uncertainty of approximately ≤ 0.04 g/100 g.

3.3.4. Saturated capillary pores

The residual water content in the capillary pores at the hydration ages of 7, 28 and 90 days for both SCMs mixtures was determined by subtracting the initial water content in the paste mixing, which was 50 g, from the sum of the water masses incorporated in crystalline, and C-(A)-S-H gel phases. As seen in Fig. 7 and Fig. 8, the remaining water in the capillary pores significantly reduces with the addition of SCMs at both cement replacement levels of 45% and 35%. At all curing ages, an increase in the natural pozzolana content at both 35% and 45% binder groups resulted in a reduction in the capillary water content. Notably, at 90 days, the alkali activated natural pozzolana mixture with 45% binder exhibited the lowest water content in the capillary pores.

Mixtures of 45% calcined clay content exhibit higher capillary water retention compared to those with 20% replacement, along with reduced gel water content at later hydration ages. This is because capillary water is calculated based on the total water mass measured in the hydrates including gel water, where lower gel water content is detected with higher calcined clay content in the hydrated pastes, this could lead to overestimating the actual water content remining in the capillary pores.

At 28 days, systems incorporating 45% natural pozzolana exhibit lower capillary water content in comparison to the 45% calcined clay systems. This could be attributed to the 7% clinker present in the natural pozzolana contributing to additional hydration and hints reducing the capillary water.

It is important to mention that each measurement technique has uncertainty limits. Consequently, when several techniques are combined, their individual errors accumulate. For the mixtures containing 35% replacement, the overall measurement uncertainty is estimated to be approximately ± 0.22 g/100 g, while for the 45% mixtures it is around ± 0.24 g/100 g. Although accurately quantifying the overall measurement error remains challenging, the water mass balance approach fulfills the purpose of presenting the water distribution in the low clinker hydrated pastes, thus enables a deeper understanding of the mechanical behavior of these systems.

4. Discussion

4.1. Water mass balance as a tool to evaluate paste volume in low-clinker binders

Fig. 10 and Fig. 11 present the calculated volume distribution across the hydrated low clinker binders at 7 and 90 days, where water associated with C-(A)-S-H gel and present in capillary pores is expressed as pore volume (cm^3/100 g binder). In addition, the volume of the empty pores formed due to the low clinker binder self-desiccation detected by chemical shrinkage measurement is also considered.

Limestone systems without the incorporation of SCMs show the highest volume of saturated capillary pores at all investigated ages, due to the limited reaction conducted in these systems [23]. Once 20% of either natural pozzolana or calcined clay are added to the mixtures, a significant reduction in the pores filled with capillary water is observed, accompanied by the progressive formation of hydrates that occupy pore spaces and further reducing the capillary porosity.

As seen in Fig. 10 and Fig. 11, increasing natural pozzolana content from 20% to 45% in the mixture with both binder groups slightly increased the calculated C-(A)-S-H gel solid volume, based on the interlayer water mass. This increment becomes more pronounced at 90 days, reflecting the continued progress of pozzolanic reactions [1]. These findings confirm that the DVS measured interlayer water in natural pozzolana systems is representing the volume of C-(A)-S-H gel layers filling the capillary spaces due to the late age pozzolanic activity. This conclusion is further supported by the observed reduction in the critical pore entry diameter in Fig. 1 and Fig. 2. In accordance, the volume of gel porosity is increasing as the capillary water amount is decreasing to form C-(A)-S-H gel layers [25,52].

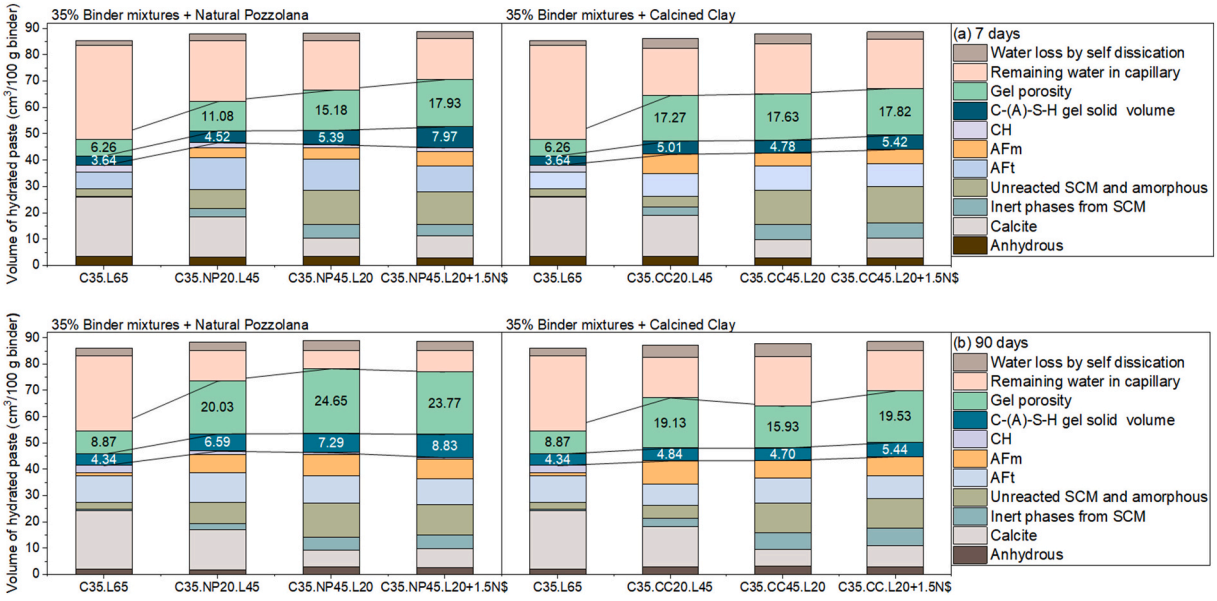

Fig. 10. Paste volume distribution (cm^3/100 g binder) of 35% binder mixtures containing reference, natural pozzolana, and calcined clay mixtures at (a) 7 days, and (b) 90 days.

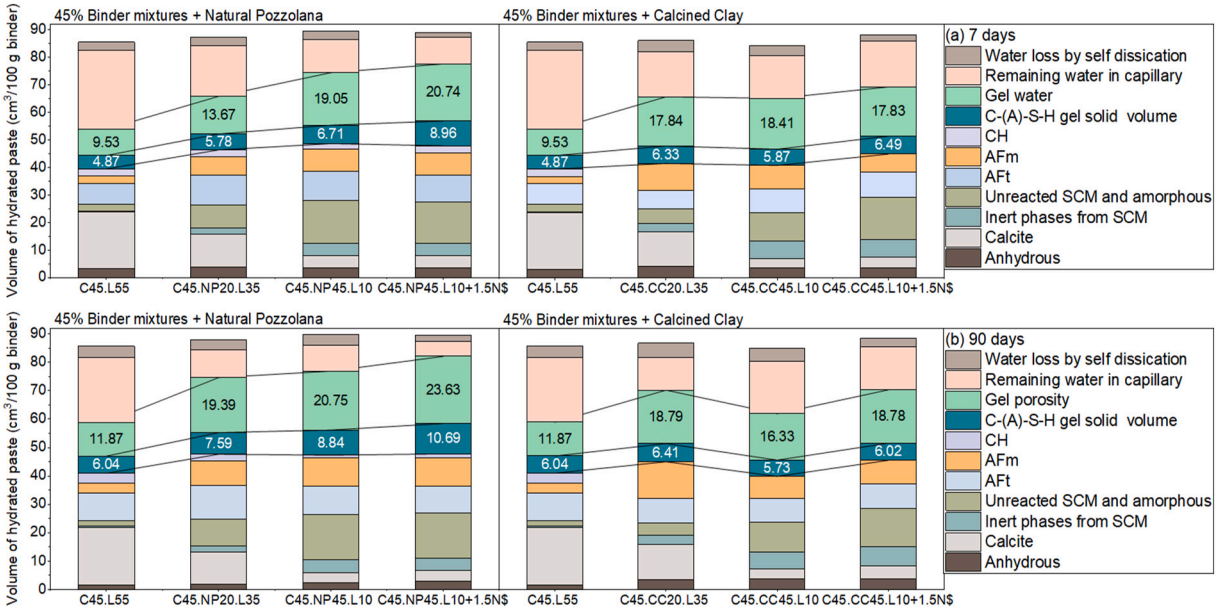

Fig. 11. Paste volume distribution (cm^3/100 g binder) of 45% binder mixtures containing reference, natural pozzolana, and calcined clay at (a) 7 days, and (b) 90 days.

In contrast, mixes containing calcined clay do not exhibit a consistent reduction in the saturated capillary porosity with increasing the calcined clay content between 7 and 90 days, as shown in Fig. 10 and Fig. 11. A higher calcined clay content accelerates early reactions, which in turn slows down the reaction rate at later ages [4,24]. As a result, saturated pores in these systems are well refined at early ages, limiting further hydrate formation, such as AFm phases. This trend is supported by Fig. 1 and Fig. 2, where mixtures containing 45% calcined clay exhibit a finer pore population from 7 days onward compared to those with natural pozzolan.

The hydration product that is most likely dominating space filling in 45% calcined clay mixes is C-(A)-S-H gel, as observed in the calcined clay desorption profiles showing water retention below 1 nm in Fig. 3 and Fig. 4. However, the estimated C-(A)-S-H gel layer volume, determined from interlayer water mass, exhibited little change. This discrepancy is attributed to the complex microstructure of low clinker systems with high calcined clay contents, where at later age variations in the C-(A)-S-H gel morphology, hydrate arrangements, and the availability of saturated space volume may influence the potential increment in the C-(A)-S-H gel layer volume, as reported in [48,53].

4.2. Correlation of pore volume estimated by water mass balance with MIP technique

Fig. 12 presents the pore volume determined using the water mass balance approach of hydrated pastes containing either limestone reference system, natural pozzolana, or calcined clay with 35% binder, compared to the total pore volume measured by MIP.

In samples containing either calcined clay or natural pozzolana, the MIP results cover the entire capillary porosity, including both saturated and emptied, as seen in Fig. 12. Additionally, MIP captures a portion of the gel porosity that is accessible to the mercury. This could be due to the interconnection between gel pores and capillary pores that are reachable through the MIP technique. This observation is consistent with findings from Muller and Scrivener [29], who successfully compared pore populations measured by ^{1}H NMR and MIP, demonstrating that MIP detects capillary pores along with a small fraction of gel porosity. The present study proposes a simpler and more accessible method for identifying pore structures and correlating them with the total porosity measured by MIP. By applying water mass balance approach, the distribution of hydration products can be illustrated, allowing for the distinction between saturated and unsaturated capillary pores and enabling assessment of the extent to which MIP captures the overall pore volume.

As illustrated in Fig. 12, limestone reference systems have a large portion of capillary pores saturated, while the gel porosity is low and inaccessible to the pressurized mercury. As a result, the total porosity measured by MIP is the highest among the studied systems. Although MIP porosity is considered to represent the capillary porosity (saturated and empty), the total capillary porosity obtained from the water mass balance exceeds the MIP value by up to approximately ±2%. This could be attributed to the measurement uncertainty.

At 90 days, the total porosity measured by MIP in mixtures with natural pozzolana is lower than at 7 days, which is related to the delayed pozzolanic reaction that contributes to the pore reduction from 7 to 90 days. In contrast, mixtures with calcined clay show only a slight reduction in total porosity between 7 and 90 days, corresponding to its higher early age reactivity.

4.3. Influence of binder composition on gel water content and microstructural refinement

The formation of gel water in hydrated pastes is facilitated by the presence of adequately sized capillary pores filled with water, as well as the absence of sulfate adsorbed on the C-(A)-S-H gel surface [25]. To gain a deeper insight into the influence of the C-(A)-S-H gel water porosity calculated from DVS desorption curves on the strength performance of the low clinker mixtures, a correlation between gel water (g/100 g binder) and total porosity % with the compressive strength of calcined clay and natural pozzolana mixtures, including reference systems, at both 7 and 90 days was conducted, as presented in Fig. 13.

At 7 and 90 days, a linear relationship was observed between the total porosity percentage reduction with the addition of natural pozzolana content in the mixtures combined by an increment in the amount of the gel water, contributed positively in the compressive strength development, which is in accordance with the findings of [25]. This observation indicates that the development in the gel water porosity plays a significant role in increasing the compressive strength of the natural pozzolana mixes, due to the formation of C-(A)-S-H gel phases and the staking of their sheets, thereby reducing the size and distribution of the pores, contributing to a denser total microstructure. However, at

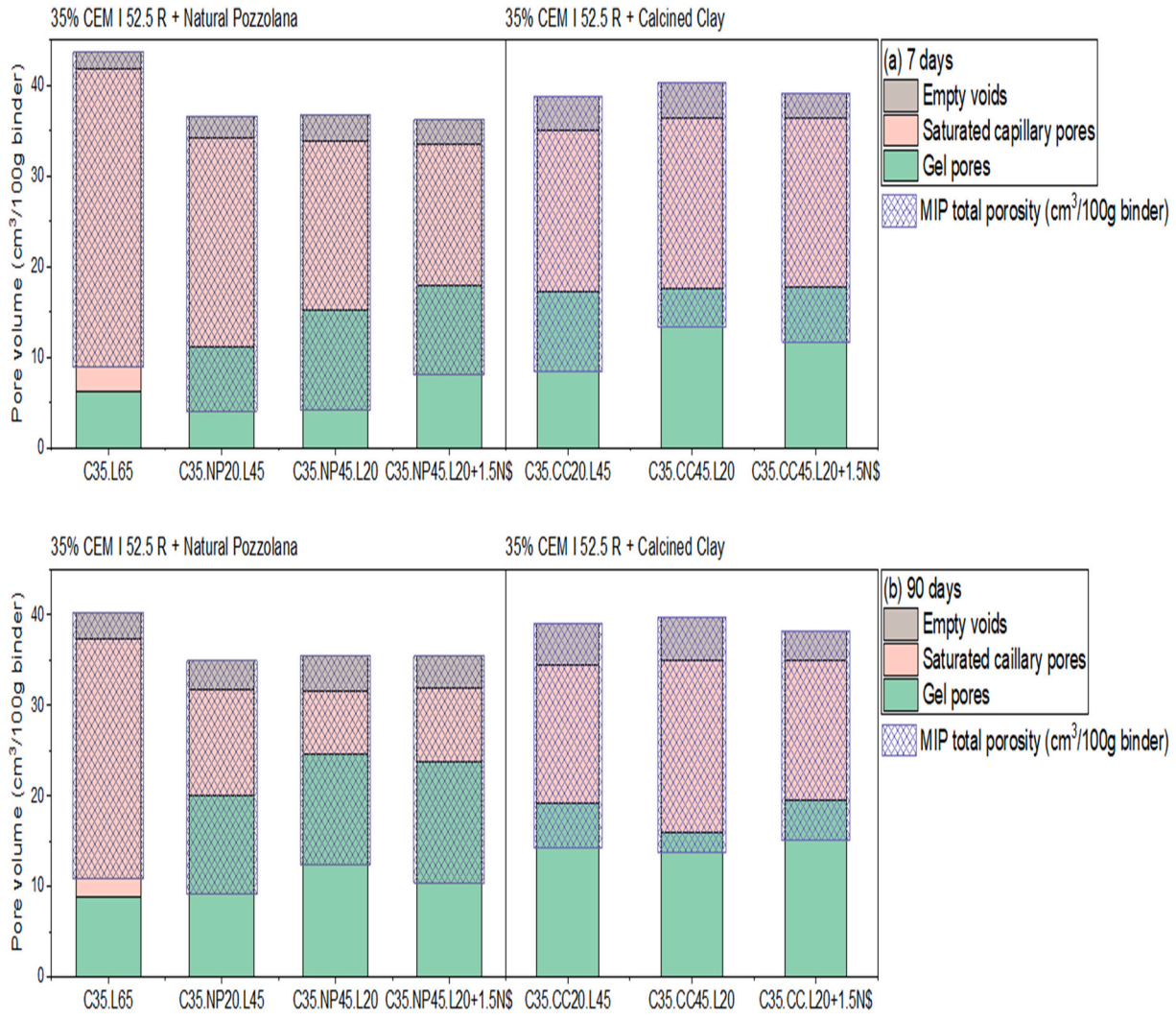

Fig. 12. Correlate pore volume of hydrated pastes of 35% binder mixtures from mass balance approach with MIP total porosity of hydration stopped samples at (a) 7 days and (b) 90 days.

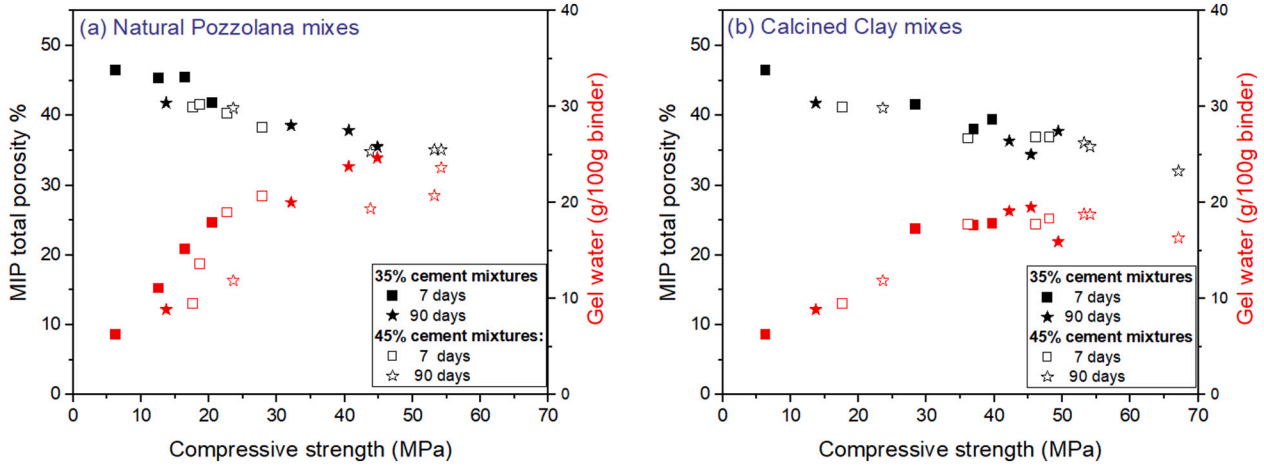

Fig. 13. Total porosity % measured by MIP technique and gel water g/100 g binder calculated from DVS as a function of the compressive strength at 7 and 90 days of (a) natural pozzolana mixes, and (b) calcined clay mixes.

90 days, natural pozzolana mixtures with 45% binder group show slightly lower gel water content than those with 35%, despite having higher compressive strength.

Regarding calcined clay mixtures, no noticeable change is observed at 7 days in gel water porosity with the addition of calcined clay in the mixture for both binder groups, while the compressive strength is increasing with higher calcined clay content. At 90 days, the mixture containing the highest calcined clay proportion exhibited the highest compressive strength but the lowest gel water content, indicating a densification in the C-(A)-S-H gel phases. This phenomena was previously explained by Muller et al. [52], where they observed a stabilization in the amount of gel water after 2 days, followed by a declination at later age. This reduction was accompanied by an increase in the crystalline and interlayer water, as detected by ^{1}H NMR technique. Therefore, they concluded that the densification of C-(A)-S-H gel occurred through its growth via the gel water, leading to a reduction in the detected gel porosity.

These observations are also made here and aligns well with the plateau of the gel water content seen in the calcined clay mixes and in the 90 days natural pozzolana mixes with higher clinker content presented in Fig. 13. This performance indicates that C-(A)-S-H gel densification is more pronounced in calcined clay mixes due to the faster depletion of capillary water [54]. Although early age strength is enhanced with the help of gel water, once compressive strength exceeds approximately 30 MPa, the densification mechanism becomes the dominant factor. Despite the variations in gel water content, both calcined clay and natural pozzolana mixes exhibit continued increases in compressive strength.

4.4. Bound water and drying weight

Another approach for validating the water mass balance is by correlating it to the mass loss of the hydrated pastes within temperature range of 40 °C to 600 °C and the bound water content calculated from TGA, which reflects the hydration products such as, crystalline phases and C-(A)-S-H gel. Bound water was calculated using the following Eq. (4) [55]:

$$\frac{W40 - W600}{W600} \quad (4)$$

Where, W40 is the mass of the sample at 40 °C and W600 is the mass at 600 °C.

Fig. 14 illustrates a comparison between the water mass balance, drying weight at 40 °C and then 600 °C, and bound water in 35% and 45% binder mixtures for the reference, natural pozzolana, and calcined clay systems at 28 days. The bound water of these systems is consistent with the water mass balance, acknowledging that some the hydrate water measured by TGA, including the crystalline water in AFt phases could be partially lost during the solvent exchange treatment used to prepare the samples prior to TGA analysis [29].

Drying weight was conducted on crushed samples, where initially the samples were placed in an oven at 40 °C until constant mass is achieved ensuring the removal of free water and some of the water associated within C-(A)-S-H gel phases, since C-(A)-S-H gel is known to be incorporated huge water content in its structure making it prone to drying [29,56]. Afterward, the samples were placed in 600 °C oven, to release the chemically bound water, and the rest of the water associated with C-(A)-S-H gel. Drying weight method is critical to the initial mass of the crushed sample and the precision of the materials handling, both of which can introduce significant measurement errors. As seen in Fig. 14, bound water is overlapping with the water loss recorded at 600 °C among all systems. The weight measured after drying at 600 °C reflects the water contents comparable to those of the crystalline water and part of the gel water and interlayer water incorporated in C-(A)-S-H gel indicated in the water mass balance of the hydrated pastes.

5. Conclusion

Water mass balance is a new approach introduced in this study to characterize the hydrates formation behavior in the low clinker binders of cement content ≤45% mixed with either highly reactive calcined clay or moderate reactive natural pozzolana. This method provides deeper understanding of the mechanism behind the strength development in these systems. The main findings in this study are:

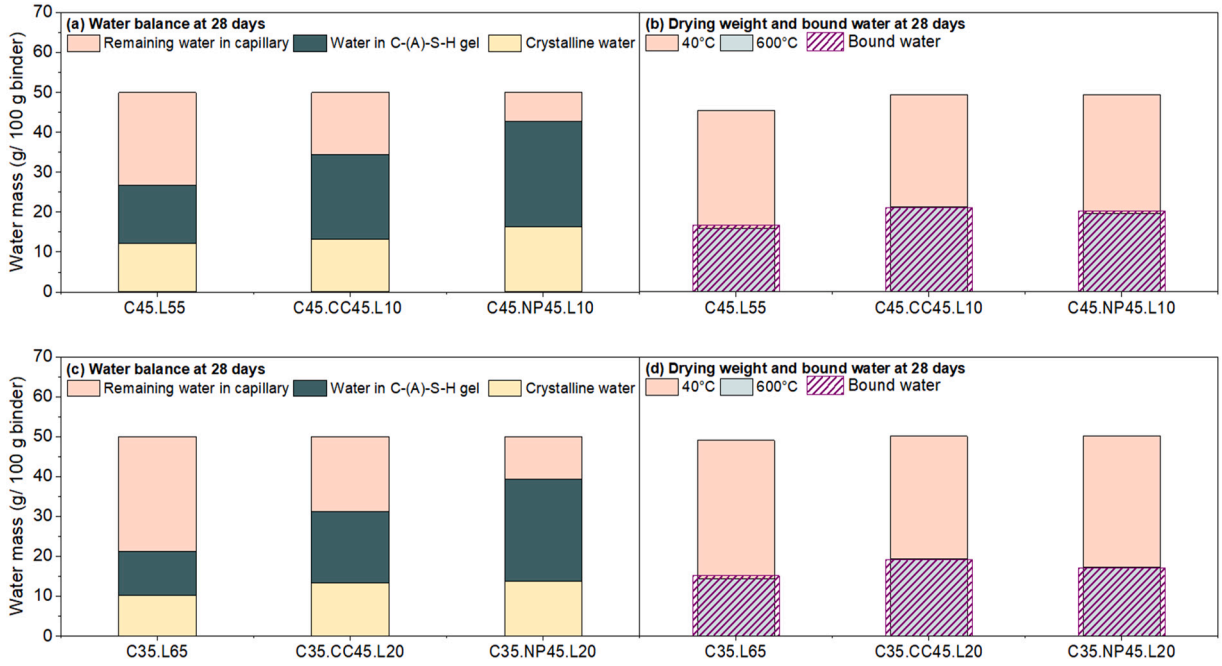

Fig. 14. A comparison between water mass balance, drying weight at 40 °C and then 600 °C, and bound water of both 45% and 35% binder mixtures of reference, natural pozzolana, and calcined clay at 28 days.

1. Combining XRD, DVS, TGA and chemical shrinkage measurements for quantifying the water amount and distribution in the hydrated low clinker binder pastes as a reflect to the porosity populations demonstrated consistent results for the studied binders.
2. The reliability of water mass balance approach is supported by the volume balance, porosity reduction measured by MIP, drying weight at 40 °C then 600 °C, as well as the bound water determined by TGA analysis of the hydrated pastes.
3. The MIP total porosity in low clinker binders incorporating either calcined clay or natural pozzolana reflects both saturated and empty capillary pores, as well as a portion of the gel porosity, an inference supported by the water mass balance distribution.
4. The interlayer and gel water contents of natural pozzolana mixtures calculated from DVS measurement reflect the quantity of C-(A)-S-H gel phases.
5. The volume of C-(A)-S-H gel layers in natural pozzolana mixtures is successfully determined by calculating the interlayer water mass using DVS technique.
6. In calcined clay mixes, the formation of densified C-(A)-S-H gel phases continues to expand within the gel water space, contributing to improvements in compressive strength.
7. The interlayer water content obtained from DVS measurement is slightly increasing in calcined clay mixtures.
8. Although fine pores in the amorphous phase of calcined clay are comparable in size to C-(A)-S-H interlayer water, as indicated by the calcined clay desorption curve, the calculated amount of water retained in these pores is too small to significantly affect the overall trend of C-(A)-S-H interlayer water.
9. Calcined clay mixtures exabit fast early reactivity, leading to occupying saturated spaces at early age, subsequently limits further C-(A)-S-H gel formation.

Water distribution data of hydrated low clinker pastes incorporating calcined clay or natural pozzolana, can be a valuable supporting tool for durability prediction and moisture transport modelling. It also provides insights into microstructural changes over time and its impact on mechanical performance.

CRediT authorship contribution statement

Aysha Anagreh: Methodology, Investigation, Formal analysis, Data curation, Conceptualization, Writing – review & editing, Writing – original draft. **Maciej Zajac:** Supervision, Conceptualization, Writing – review & editing. **Mohsen Ben Haha:** Supervision, Formal analysis, Conceptualization. **Arnaud Muller:** Supervision, Data curation, Conceptualization, Writing – review & editing. **Fabien Georget:** Supervision, Formal analysis, Writing – review & editing. **Thomas Matschei:** Supervision, Formal analysis.

Declaration of competing interest

The authors declare that they have no known competing financial interests or personal relationships that could have appeared to influence the work reported in this paper.

Acknowledgement

We sincerely thank Ana Costa for the insightful discussions. Our gratitude goes to the ANC laboratory colleagues for their significant contributions and engagement. During the preparation of this work the authors used Microsoft Copilot in language refinement, specifically for rephrasing sentences to improve clarity and readability. After using this tool, the authors reviewed and edited the content as needed and take full responsibility for the content of the published article.

Appendix A

Table 6
Calculated free water from water mass balance approach at 7, 28, and 90 days.

Mixtures	Free water calculated from water mass balance including capillary and gel water			Free water calculated from TGA		
	7 days	28 days	90 days	7 days	28 days	90 days
C35.L65	41.84	37.61	37.37	38.54	34.88	33.09
C35.NP20.L45	34.12	32.92	31.68	35.00	33.54	32.06
C35.NP45.L20	33.89	33.07	31.55	33.83	32.83	30.01
C35.NP45.L20 + 1.5 N$	33.49	31.41	31.94	34.87	33.15	29.38
C45.L55	38.09	35.17	34.73	33.82	33.34	29.79
C45.NP20.L35	32.06	29.74	29.01	32.93	30.40	30.35
C45.NP45.L10	31.08	29.88	29.77	32.65	29.71	29.26
C45.NP45.L10 + 1.5 N$	30.39	28.89	28.96	33.37	31.40	30.11
C35.CC20.L45	35.09	33.57	34.45	32.04	31.90	30.82
C35.CC45.L20	36.50	34.50	34.87	31.51	30.86	28.14
C35.CC45.L20 + 1.5 N$	36.35	35.08	34.95	31.58	32.02	31.51
C45.CC20.L35	34.14	31.80	30.16	30.11	29.32	28.60
C45.CC45.L10	33.84	34.25	34.65	30.80	28.91	27.91
C45.CC45.L10 + 1.5 N$	34.46	33.69	33.89	31.48	30.25	29.06

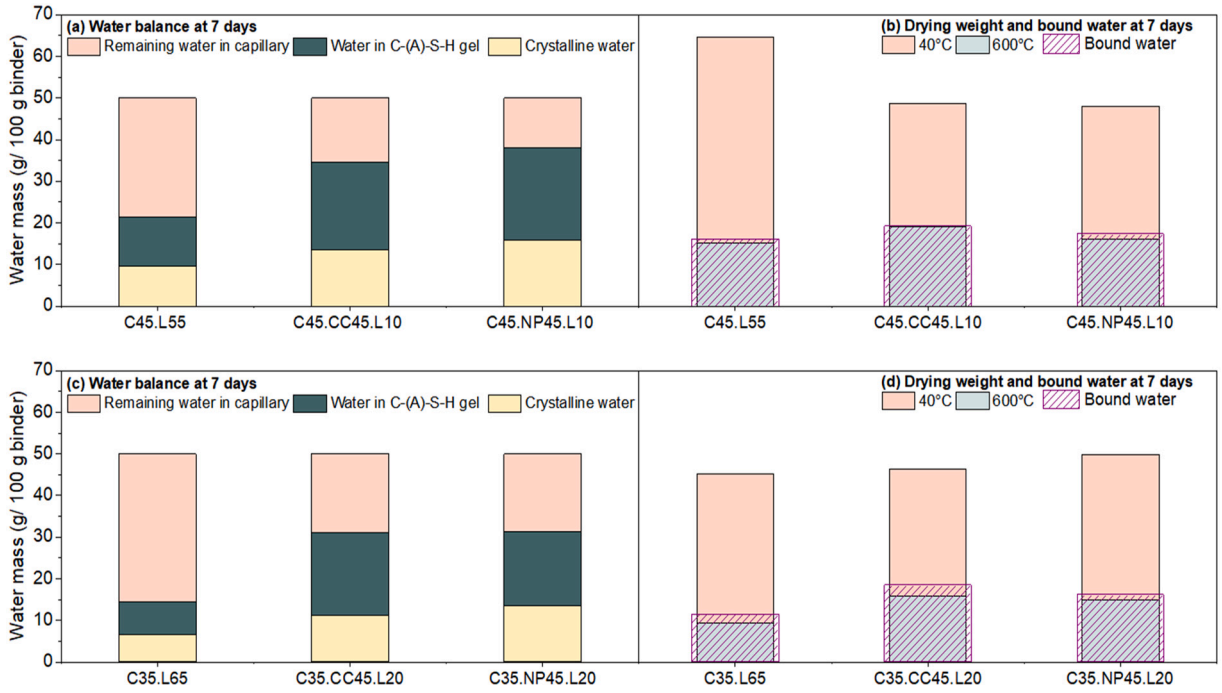

Fig. 15. A comparison between water mass balance, drying weight at 40 °C and then 600 °C, and bound water of both 45% and 35% binder mixtures of reference, natural pozzolana, and calcined clay at 7 days.

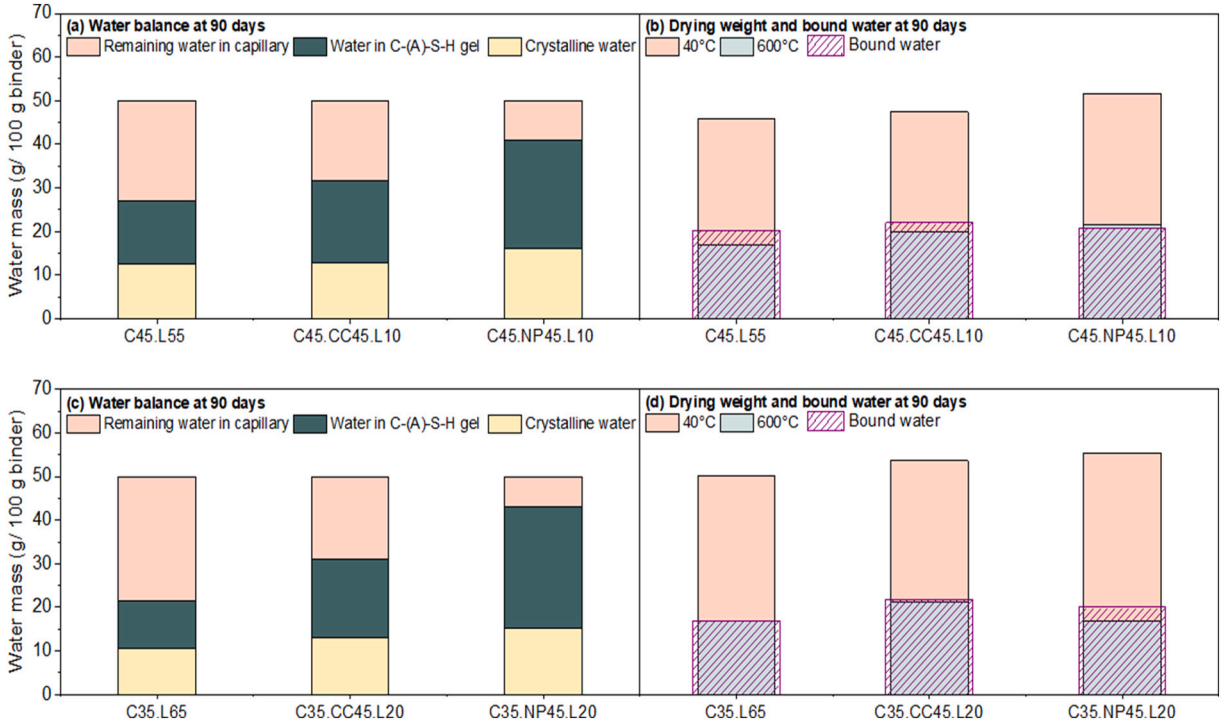

Fig. 16. A comparison between water mass balance, drying weight at 40 °C and then 600 °C, and bound water of both 45% and 35% binder mixtures of reference, natural pozzolana, and calcined clay at 90 days.

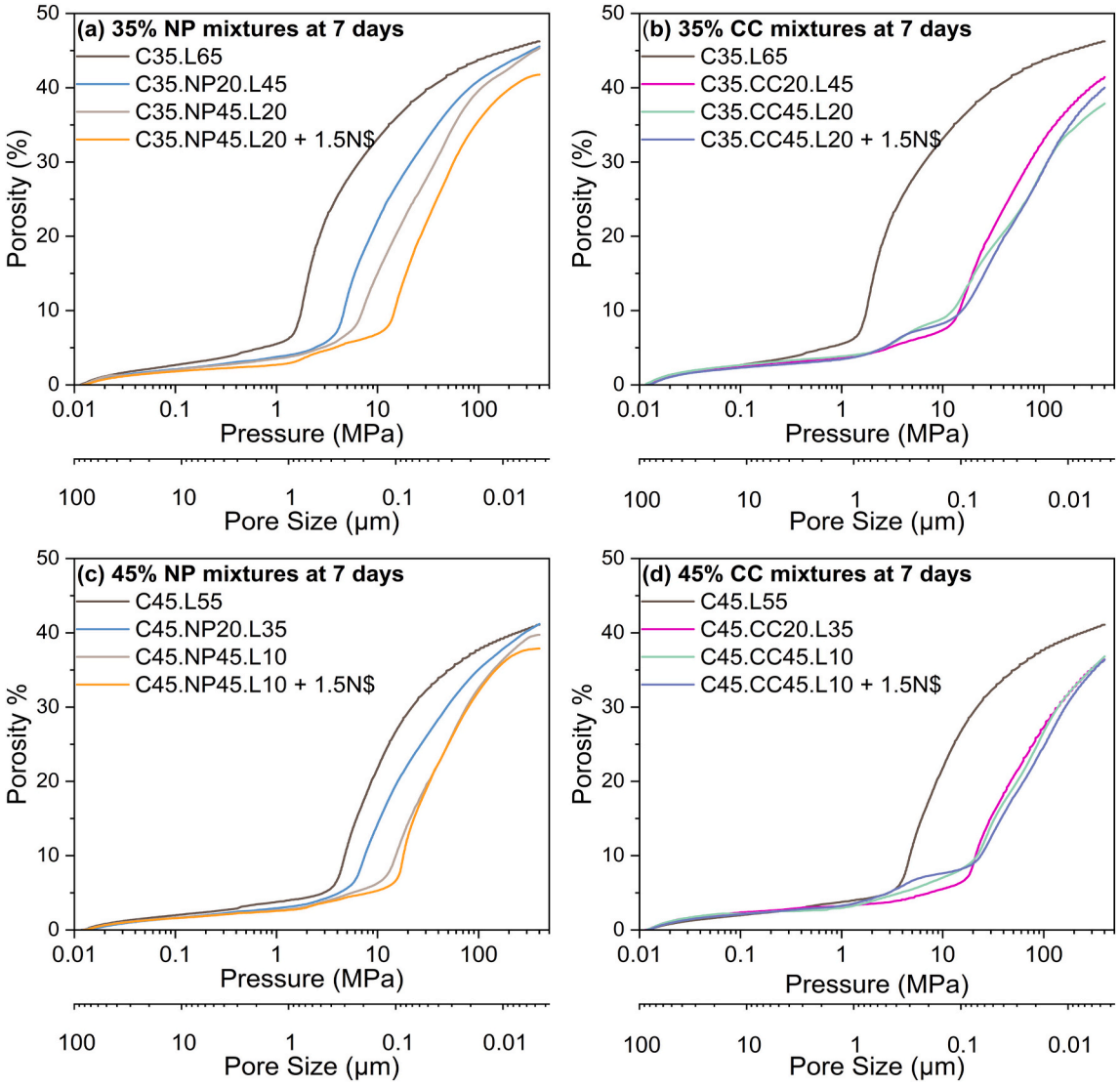

Fig. 17. Cumulative MIP porosity as a function of increased pressure at 7 days for (a) 35% mixtures containing natural pozzolana, (b) 35% mixtures with calcined clay, (c) 45% mixtures containing natural pozzolana, and (d) 45% mixtures containing calcined clay.

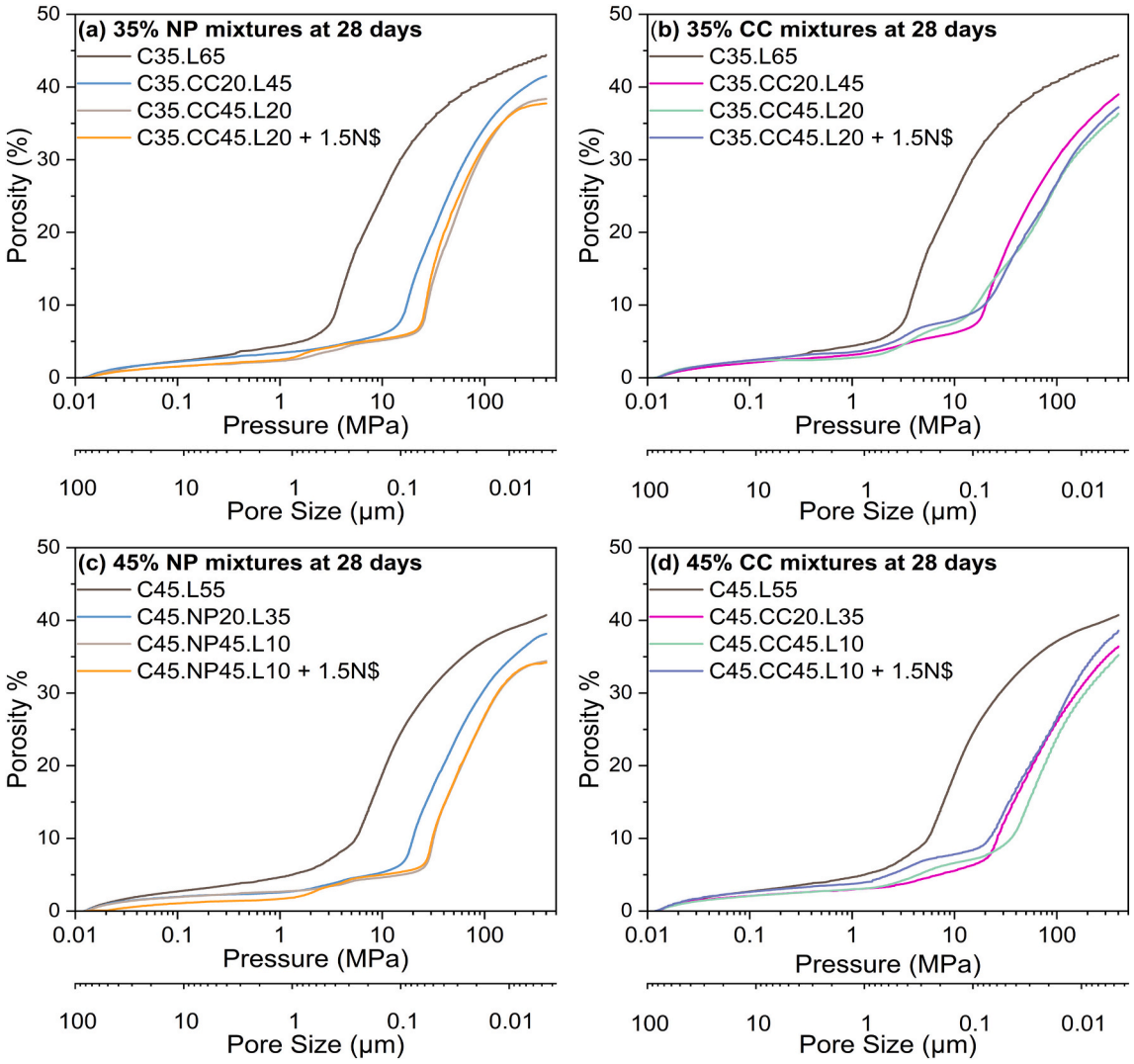

Fig. 18. Cumulative MIP porosity as a function of increased pressure at 28 days for (a) 35% mixtures containing natural pozzolana, (b) 35% mixtures with calcined clay, (c) 45% mixtures with natural pozzolana, and (d) 45% mixtures with calcined clay.

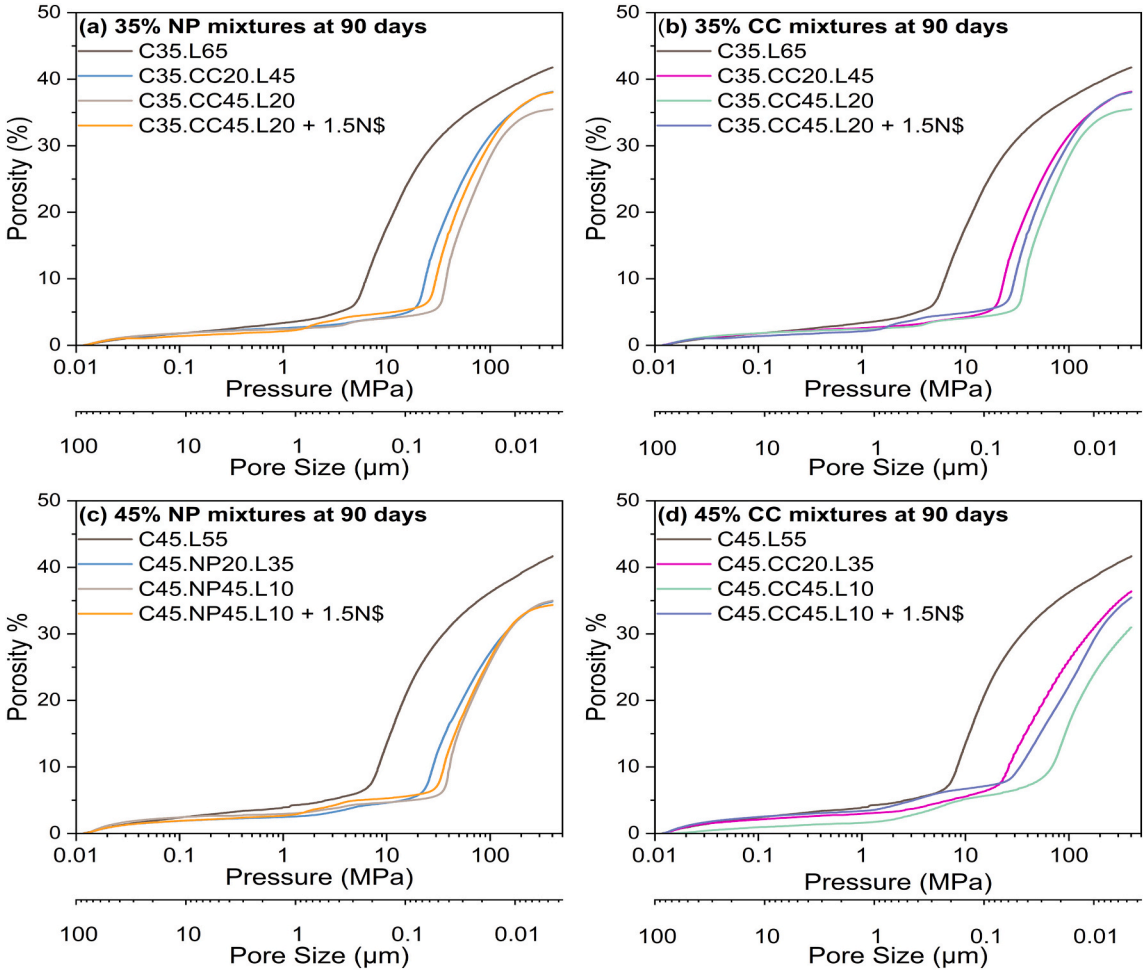

Fig. 19. Cumulative MIP porosity as a function of increased pressure at 90 days for (a) 35% mixtures containing natural pozzolana, (b) 35% mixtures with calcined clay, (c) 45% mixtures with natural pozzolana, and (d) 45% mixtures containing calcined clay.

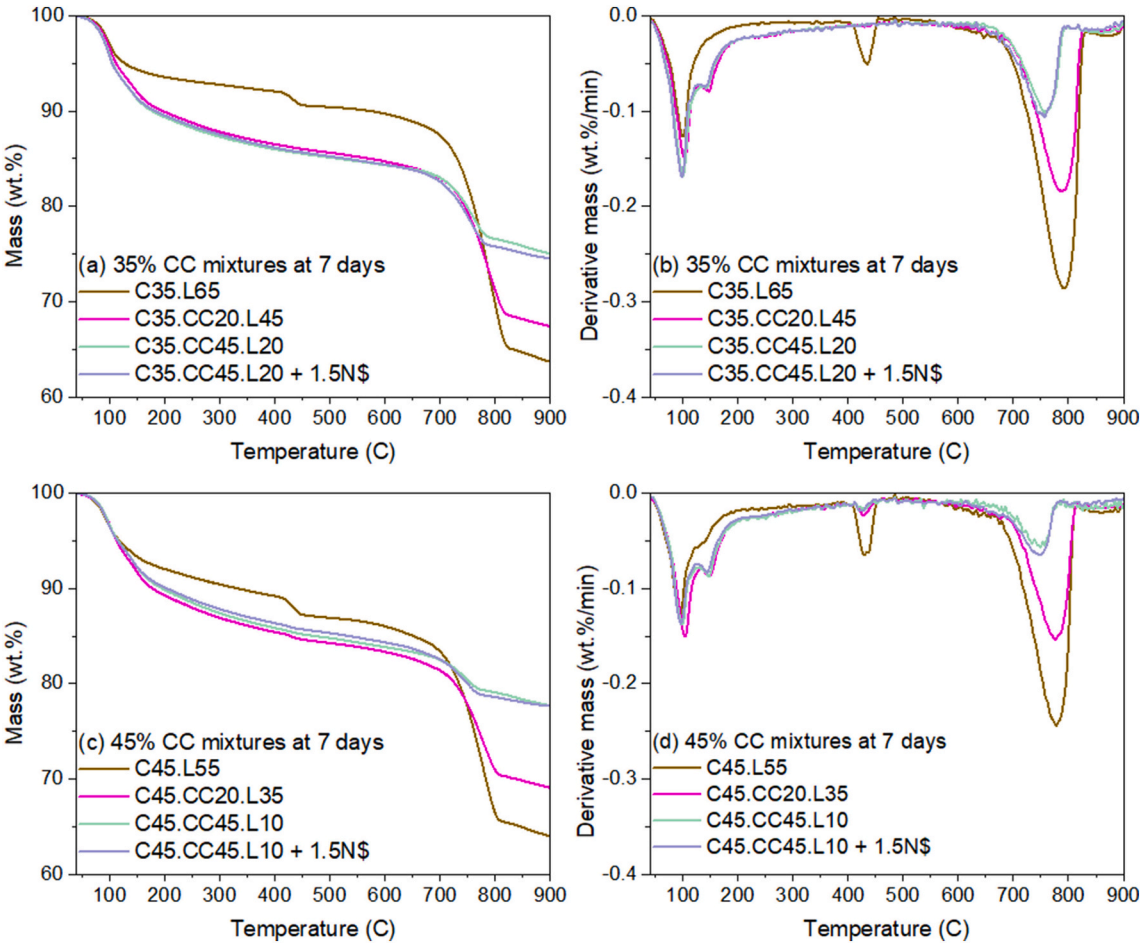

Fig. 20. Thermogravimetric (TGA) and derivative thermogravimetric (DTG) curves of calcined clay mixtures at 7 days for the 35% mixtures (a and b) and 45% mixtures (c and d).

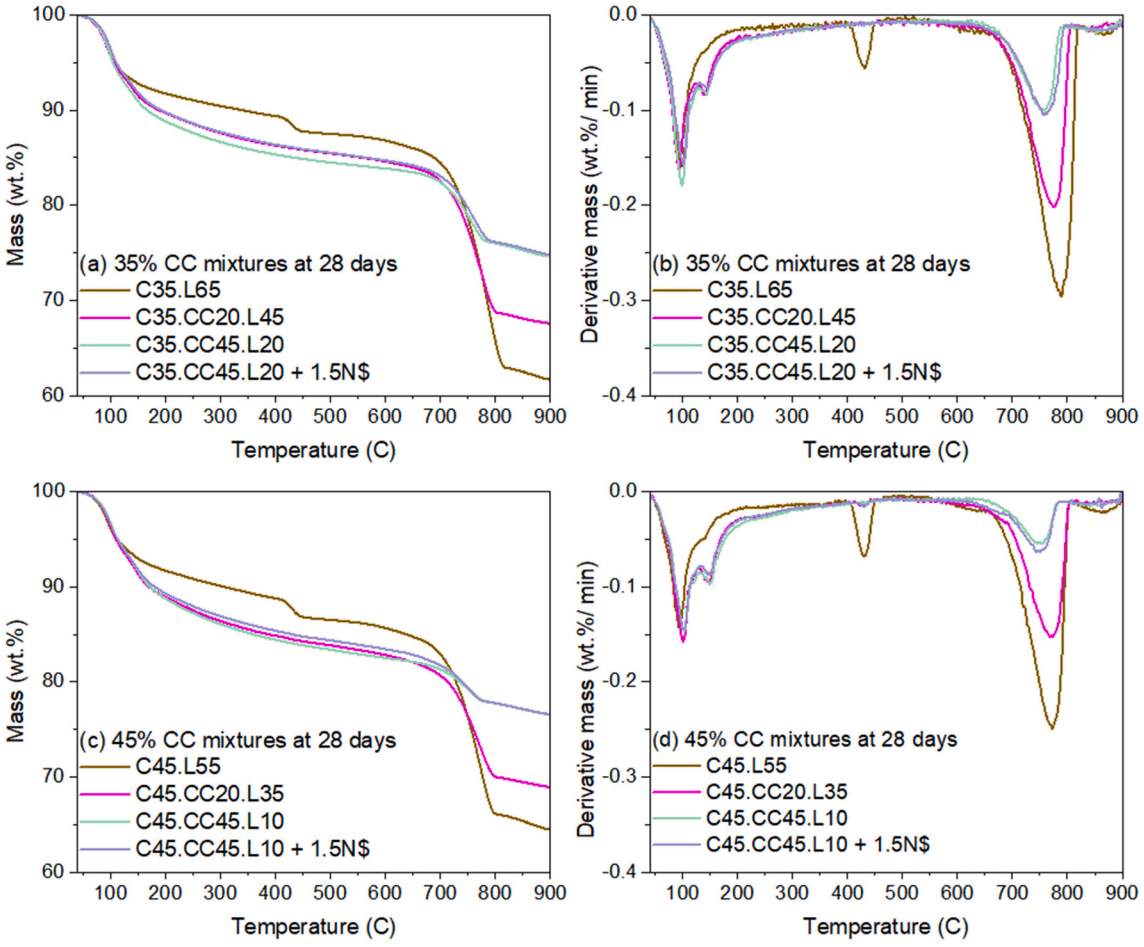

Fig. 21. Thermogravimetric (TGA) and derivative thermogravimetric (DTG) curves of calcined clay mixtures at 28 days for the 35% mixtures (a and b) and 45% mixtures (c and d).

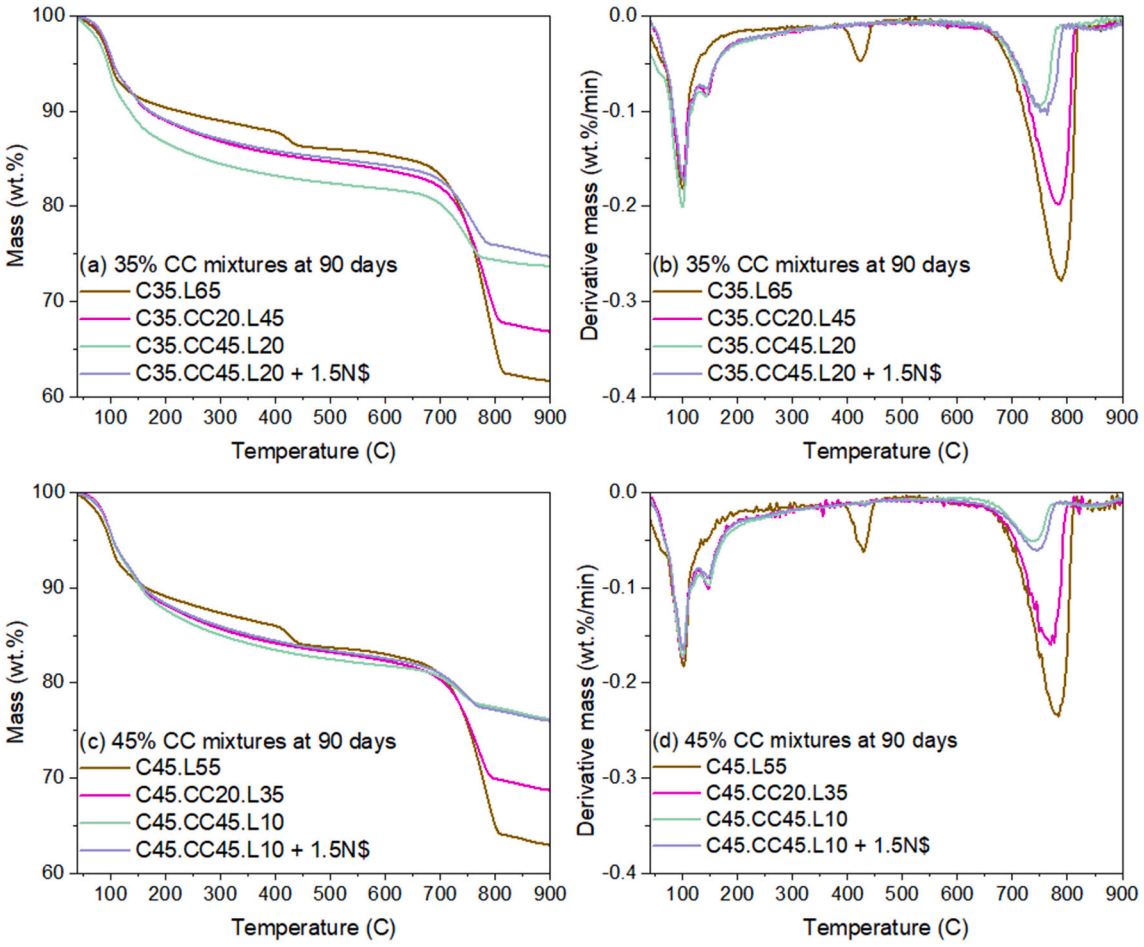

Fig. 22. Thermogravimetric (TGA) and derivative thermogravimetric (DTG) curves of calcined clay mixtures at 90 days for the 35% mixtures (a and b) and 45% mixtures (c and d).

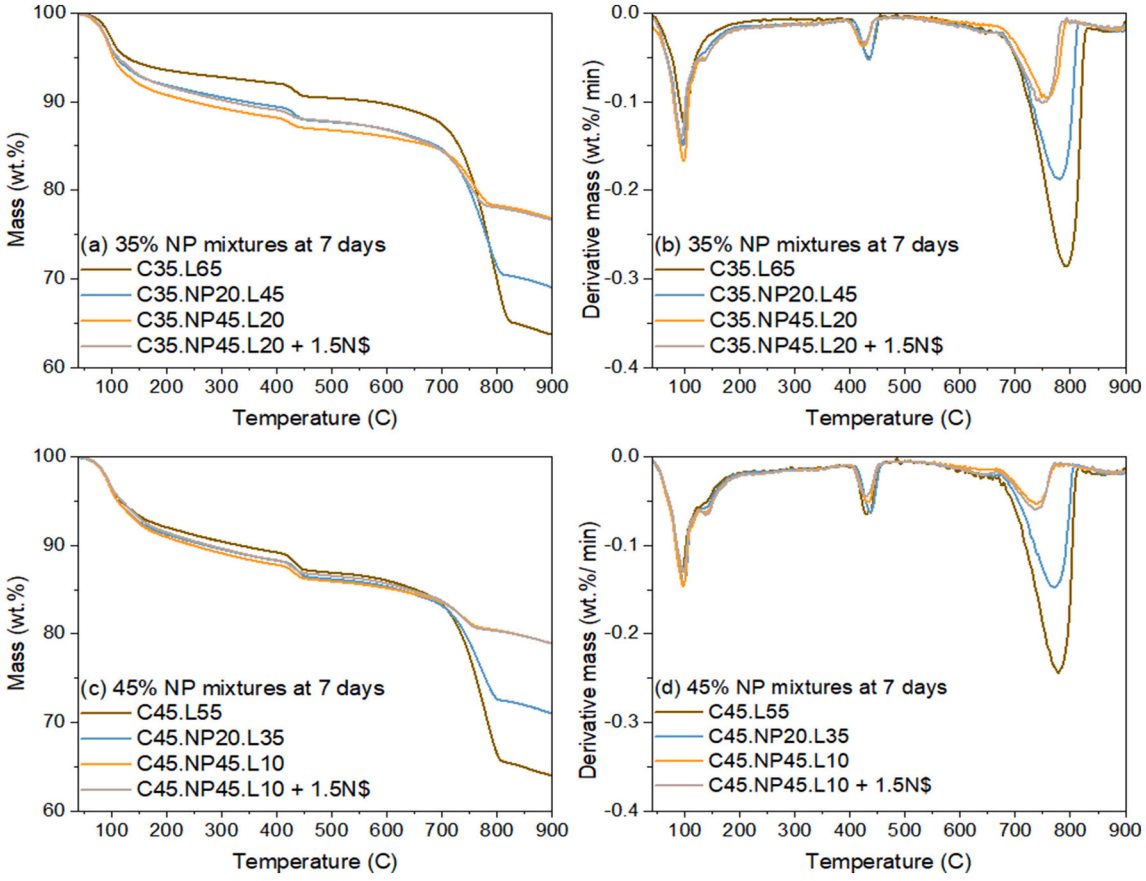

Fig. 23. Thermogravimetric (TGA) and derivative thermogravimetric (DTG) curves of natural pozzolana mixtures at 7 days for the 35% mixtures (a and b) and 45% mixtures (c and d).

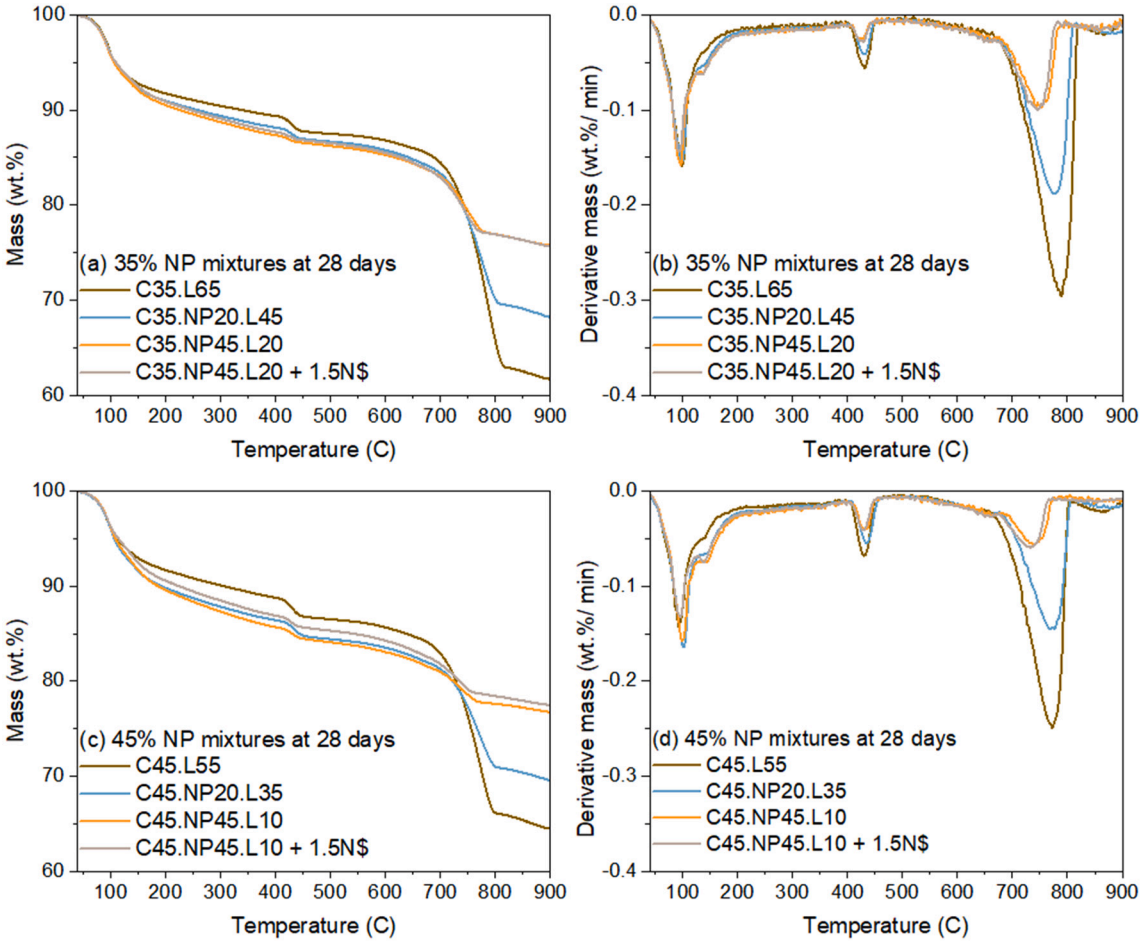

Fig. 24. Thermogravimetric (TGA) and derivative thermogravimetric (DTG) curves of natural pozzolana mixtures at 28 days for the 35% mixtures (a and b) and 45% mixtures (c and d).

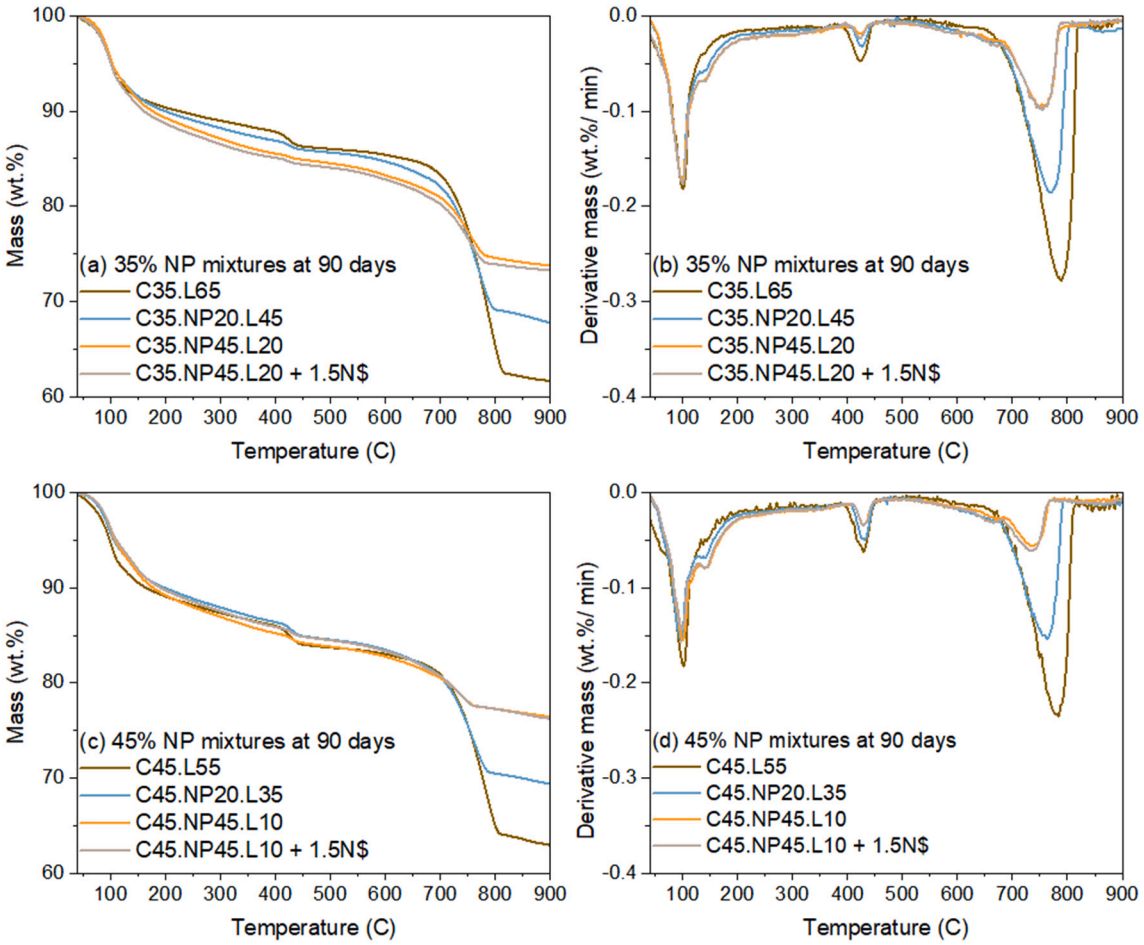

Fig. 25. Thermogravimetric (TGA) and derivative thermogravimetric (DTG) curves of natural pozzolana mixtures at 90 days for the 35% mixtures (a and b) and 45% mixtures (c and d).

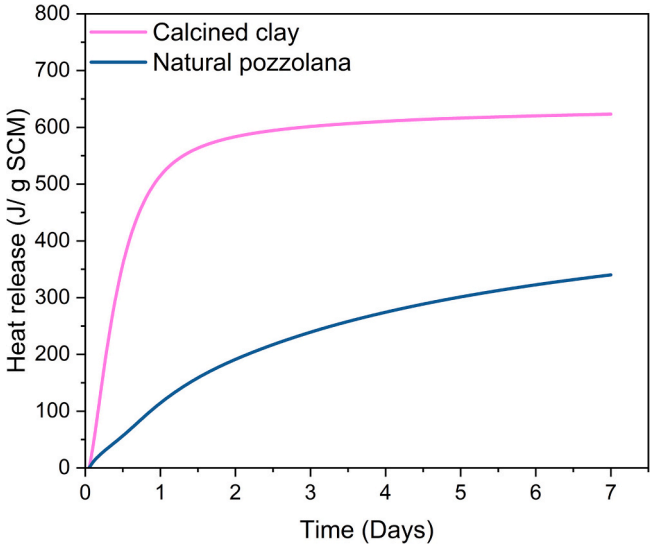

Fig. 26. Reactivity of calcined clay and natural pozzolana materials determined using the R^3 heat release test.

Data availability

Data will be made available on request.

References

[1] M. Ben Haha, P. Termkhajornkit, A. Ouzia, S. Uppalapati, B. Huet, Low clinker systems - towards a rational use of SCMs for optimal performance, Cem. Concr. Res. 174 (2023) 107312, https://doi.org/10.1016/j.cemconres.2023.107312.

[2] K.L. Scrivener, V.M. John, E.M. Gartner, Eco-efficient cements: potential economically viable solutions for a low-CO2 cement-based materials industry, Cem. Concr. Res. 114 (2018) 2–26, https://doi.org/10.1016/j.cemconres.2018.03.015.

[3] F. Zunino, Y. Dhandapani, M. Ben Haha, J. Skibsted, S. Joseph, S. Krishnan, A. Parashar, M.C.G. Juenger, T. Hanein, S.A. Bernal, K.L. Scrivener, F. Avet, Hydration and mixture design of calcined clay blended cements: review by the RILEM TC 282-CCL, Mater. Struct. 55 (9) (2022), https://doi.org/10.1617/s11527-022-02060-1.

[4] F. Avet, K. Scrivener, Investigation of the calcined kaolinite content on the hydration of limestone calcined clay cement (LC3), Cem. Concr. Res. 107 (2018) 124–135, https://doi.org/10.1016/j.cemconres.2018.02.016.

[5] G. Habert, N. Choupay, J.M. Montel, D. Guillaume, G. Escadeillas, Effects of the secondary minerals of the natural pozzolans on their pozzolanic activity, Cem. Concr. Res. 38 (7) (2008) 963–975, https://doi.org/10.1016/j.cemconres.2008.02.005.

[6] J. Skibsted, R. Snellings, Reactivity of supplementary cementitious materials (SCMs) in cement blends, Cem. Concr. Res. 124 (2019) 105799, https://doi.org/10.1016/j.cemconres.2019.105799.

[7] F. Massazza, Pozzolanic cements, Cem. Concr. Compos. 15 (1993) 185–214.

[8] M. Ghrici, S. Kenai, M. Said-Mansour, Mechanical properties and durability of mortar and concrete containing natural pozzolana and limestone blended cements, Cem. Concr. Compos. 29 (7) (2007) 542–549, https://doi.org/10.1016/j.cemconcomp.2007.04.009.

[9] I. Diaz-Loya, M. Juenger, S. Seraj, R. Minkara, Extending supplementary cementitious material resources: reclaimed and remediated fly ash and natural pozzolans, Cem. Concr. Compos. 101 (2019) 44–51, https://doi.org/10.1016/j.cemconcomp.2017.06.011.

[10] J. Fu, A.M. Jones, M.W. Bligh, C. Holt, L.M. Keyte, F. Moghaddam, S.J. Foster, T. D. Waite, Mechanisms of enhancement in early hydration by sodium sulfate in a slag-cement blend – insights from pore solution chemistry, Cem. Concr. Res. 135 (2020) 106110, https://doi.org/10.1016/j.cemconres.2020.106110.

[11] B. Mota, T. Matschei, K. Scrivener, The influence of sodium salts and gypsum on alite hydration, Cem. Concr. Res. 75 (2015) 53–65, https://doi.org/10.1016/j.cemconres.2015.04.015.

[12] A. Kumar, G. Sant, C. Patapy, C. Gianocca, K.L. Scrivener, The influence of sodium and potassium hydroxide on alite hydration: experiments and simulations, Cem. Concr. Res. 42 (11) (2012) 1513–1523, https://doi.org/10.1016/j.cemconres.2012.07.003.

[13] M. Zhang, F. Zunino, L. Yang, F. Wang, K. Scrivener, Understanding the negative effects of alkalis on long-term strength of Portland cement, Cem. Concr. Res. 174 (2023) 107348, https://doi.org/10.1016/j.cemconres.2023.107348.

[14] B. Lothenbach, K. Scrivener, R.D. Hooton, Supplementary cementitious materials, Cem. Concr. Res. 41 (12) (2011) 1244–1256, https://doi.org/10.1016/j.cemconres.2010.12.001.

[15] M. Auroy, S. Poyet, P. Le Bescop, J.-M. Torrenti, T. Charpentier, M. Moskura, X. Bourbon, Comparison between natural and accelerated carbonation (3% CO2): impact on mineralogy, microstructure, water retention and cracking, Cem. Concr. Res. 109 (2018) 64–80, https://doi.org/10.1016/j.cemconres.2018.04.012.

[16] M. Auroy, S. Poyet, P. Le Bescop, J.-M. Torrenti, T. Charpentier, M. Moskura, X. Bourbon, Impact of carbonation on unsaturated water transport properties of cement-based materials, Cem. Concr. Res. 74 (2015) 44–58, https://doi.org/10.1016/j.cemconres.2015.04.002.

[17] A. Morandeau, M. Thiéry, P. Dangla, Impact of accelerated carbonation on OPC cement paste blended with fly ash, Cem. Concr. Res. 67 (2015) 226–236, https://doi.org/10.1016/j.cemconres.2014.10.003.

[18] A. Morandeau, M. Thiéry, P. Dangla, Investigation of the carbonation mechanism of CH and C-S-H in terms of kinetics, microstructure changes and moisture properties, Cem. Concr. Res. 56 (2014) 153–170, https://doi.org/10.1016/j.cemconres.2013.11.015.

[19] K.L. Scrivener, T. Matschei, F. Georget, P. Juilland, A.K. Mohamed, Advances in hydration and thermodynamics of cementitious systems, Cem. Concr. Res. 174 (2023) 107332, https://doi.org/10.1016/j.cemconres.2023.107332.

[20] O. Linderoth, L. Wadsö, D. Jansen, Long-term cement hydration studies with isothermal calorimetry, Cem. Concr. Res. 141 (2021) 106344, https://doi.org/10.1016/j.cemconres.2020.106344.

[21] F. Zunino, K. Scrivener, The reaction between metakaolin and limestone and its effect in porosity refinement and mechanical properties, Cem. Concr. Res. 140 (2021) 106307, https://doi.org/10.1016/j.cemconres.2020.106307.

[22] Y. Briki, F. Avet, M. Zajac, P. Bowen, M.B. Haha, K. Scrivener, Understanding of the factors slowing down metakaolin reaction in limestone calcined clay cement (LC3) at late ages, Cem. Concr. Res. 146 (2021) 106477, https://doi.org/10.1016/j.cemconres.2021.106477.

[23] F. Georget, S. Sui, W. Wilson, K.L. Scrivener, Reconciliation of pore structure characterization methods: the simple case of PC-limestone cement pastes, Cem. Concr. Res. 184 (2024) 107624, https://doi.org/10.1016/j.cemconres.2024.107624.

[24] F. Zunino, K. Scrivener, Microstructural developments of limestone calcined clay cement (LC3) pastes after long-term (3 years) hydration, Cem. Concr. Res. 153 (2022) 106693, https://doi.org/10.1016/j.cemconres.2021.106693.

[25] E.M.J. Bérodier, A.C.A. Muller, K.L. Scrivener, Effect of sulfate on C-S-H at early age, Cem. Concr. Res. 138 (2020) 106248, https://doi.org/10.1016/j.cemconres.2020.106248.

[26] A.C.A. Muller, K.L. Scrivener, A.M. Gajewicz, P.J. McDonald, Use of bench-top NMR to measure the density, composition and desorption isotherm of C–S–H in cement paste, Microporous Mesoporous Mater. 178 (2013) 99–103, https://doi.org/10.1016/j.micromeso.2013.01.032.

[27] M. Rastogi, A. Müller, M.B. Haha, K.L. Scrivener, The role of cavitation in drying cementitious materials, Cem. Concr. Res. 154 (2022) 106710, https://doi.org/10.1016/j.cemconres.2022.106710.

[28] R.A. Cook, K.C. Hover, Mercury porosimetry of hardened cement pastes, Cem. Concr. Res. 29 (6) (1999) 933–943, https://doi.org/10.1016/S0008-8846(99)00083-6.

[29] A.C.A. Muller, K.L. Scrivener, A reassessment of mercury intrusion porosimetry by comparison with 1H NMR relaxometry, Cem. Concr. Res. 100 (2017) 350–360, https://doi.org/10.1016/j.cemconres.2017.05.024.

[30] M. Wyrzykowski, P.J. McDonald, K.L. Scrivener, P. Lura, Water redistribution within the microstructure of cementitious materials due to temperature changes studied with ^{1}H NMR, J. Phys. Chem. C 121 (50) (2017) 27950–27962, https://doi.org/10.1021/acs.jpcc.7b08141.

[31] Z. Yu, R. De Oliveira-Silva, Y. Pontikes, D. Sakellariou, Low-field 1H NMR study on geopolymers: the effect of paramagnetic Fe(III), Cem. Concr. Res. 166 (2023) 107116, https://doi.org/10.1016/j.cemconres.2023.107116.

[32] I. Maruyama, J. Rymeš, M. Vandamme, B. Coasne, Cavitation of water in hardened cement paste under short-term desorption measurements, Mater. Struct. 51 (6) (2018) 159, https://doi.org/10.1617/s11527-018-1285-x.

[33] D. Snoeck, L.F. Velasco, A. Mignon, S. Van Vlierberghe, P. Dubruel, P. Lodewyckx, N. De Belie, The influence of different drying techniques on the water sorption properties of cement-based materials, Cem. Concr. Res. 64 (2014) 54–62, https://doi.org/10.1016/j.cemconres.2014.06.009.

[34] M. Wu, B. Johannesson, M. Geiker, Application of water vapor sorption measurements for porosity characterization of hardened cement pastes, Constr. Build. Mater. 66 (2014) 621–633, https://doi.org/10.1016/j.conbuildmat.2014.06.004.

[35] V. Baroghel-Bouny, Water vapour sorption experiments on hardened cementitious materials, Cem. Concr. Res. 37 (3) (2007) 414–437, https://doi.org/10.1016/j.cemconres.2006.11.019.

[36] N. Alderete, Y. Villagrán, A. Mignon, D. Snoeck, N. De Belie, Pore structure description of mortars containing ground granulated blast-furnace slag by mercury intrusion porosimetry and dynamic vapour sorption, Constr. Build. Mater. 145 (2017) 157–165, https://doi.org/10.1016/j.conbuildmat.2017.03.245.

[37] F. Georget, W. Wilson, K.L. Scrivener, Edxia: microstructure characterisation from quantified SEM-EDS hypermaps, Cem. Concr. Res. 141 (2021) 106327, https://doi.org/10.1016/j.cemconres.2020.106327.

[38] F. Avet, R. Snellings, A. Alujas Diaz, M. Ben Haha, K. Scrivener, Development of a new rapid, relevant and reliable (R3) test method to evaluate the pozzolanic reactivity of calcined kaolinitic clays, Cem. Concr. Res. 85 (2016) 1–11, https://doi.org/10.1016/j.cemconres.2016.02.015.

[39] TOPAS V6.0, General Profile and Structure Analysis Software for Powder Diffraction Data, Users's Manual, Bruker AXS, Karlsruhe, 2017.

[40] H. Chen, M. Wyrzykowski, K. Scrivener, P. Lura, Prediction of self-desiccation in low water-to-cement ratio pastes based on pore structure evolution, Cem. Concr. Res. 49 (2013) 38–47, https://doi.org/10.1016/j.cemconres.2013.03.013.

[41] F. Avet, X. Li, K. Scrivener, Determination of the amount of reacted metakaolin in calcined clay blends, Cem. Concr. Res. 106 (2018) 40–48, https://doi.org/10.1016/j.cemconres.2018.01.009.

[42] M. Balonis, F.P. Glasser, The density of cement phases, Cem. Concr. Res. 39 (9) (2009) 733–739, https://doi.org/10.1016/j.cemconres.2009.06.005.

[43] Mindat.org, Olivine Mineral Data, 2000. Available at: https://www.mindat.org. (Accessed 11 July 2025).

[44] Mindat.Org, Mineral information and data, Available at: https://www.mindat.org, 2000. (Accessed 11 July 2025).

[45] Muller, A. C. A., Characterization of porosity & C-S-H in Cement Pastes by 1H NMR (n.d.).

[46] B. Mota, T. Matschei, K. Scrivener, Impact of NaOH and Na2SO4 on the kinetics and microstructural development of white cement hydration, Cem. Concr. Res. 108 (2018) 172–185, https://doi.org/10.1016/j.cemconres.2018.03.017.

[47] P.T. Durdziński, M. Ben Haha, M. Zajac, K.L. Scrivener, Phase assemblage of composite cements, Cem. Concr. Res. 99 (2017) 172–182, https://doi.org/10.1016/j.cemconres.2017.05.009.

[48] M. Zajac, J. Skocek, S. Adu-Amankwah, L. Black, M. Ben Haha, Impact of microstructure on the performance of composite cements: why higher total porosity can result in higher strength, Cem. Concr. Compos. 90 (2018) 178–192, https://doi.org/10.1016/j.cemconcomp.2018.03.023.

[49] L. Ferrari, A. Nagmutdinova, A. Müller, N. Mikanovic, M. Ben-Haha, V. Bortolotti, E. Franzoni, Water Retention in Calcined Clay: A Key Factor in the Rheological Challenges of Cement Mixtures, 2024, https://doi.org/10.2139/ssrn.5035709.

[50] M. Cisiński, G. Biava, F. Winnefeld, Ł. Sadowski, M. Ben Haha, M. Zajac, Carbonated calcium silicates as pozzolanic supplementary cementitious materials, Constr. Build. Mater. 443 (2024) 137764, https://doi.org/10.1016/j.conbuildmat.2024.137764.

[51] M. Antoni, J. Rossen, F. Martirena, K. Scrivener, Cement substitution by a combination of metakaolin and limestone, Cem. Concr. Res. 42 (12) (2012) 1579–1589, https://doi.org/10.1016/j.cemconres.2012.09.006.
[52] A.C.A. Muller, K.L. Scrivener, A.M. Gajewicz, P.J. McDonald, Densification of C–S–H measured by^{1} H NMR relaxometry, J. Phys. Chem. C 117 (1) (2013) 403–412, https://doi.org/10.1021/jp3102964.
[53] M. Zajac, P. Durdzinski, Z. Giergiczny, M. Ben Haha, New insights into the role of space on the microstructure and the development of strength of multicomponent cements, Cem. Concr. Compos. 121 (2021) 104070, https://doi.org/10.1016/j.cemconcomp.2021.104070.
[54] E. Masoero, G. Cusatis, G. Di Luzio, C–S–H gel densification: the impact of the nanoscale on self-desiccation and sorption isotherms, Cem. Concr. Res. 109 (2018) 103–119, https://doi.org/10.1016/j.cemconres.2018.04.014.
[55] K. De Weerdt, M.B. Haha, G. Le Saout, K.O. Kjellsen, H. Justnes, B. Lothenbach, Hydration mechanisms of ternary Portland cements containing limestone powder and fly ash, Cem. Concr. Res. 41 (3) (2011) 279–291, https://doi.org/10.1016/j.cemconres.2010.11.014.
[56] M.C. Garci Juenger, H.M. Jennings, Examining the relationship between the microstructure of calcium silicate hydrate and drying shrinkage of cement pastes, Cem. Concr. Res. 32 (2) (2002) 289–296, https://doi.org/10.1016/S0008-8846(01)00673-1.